Nanotechnologies for Noninvasive Measurement of Drug Release
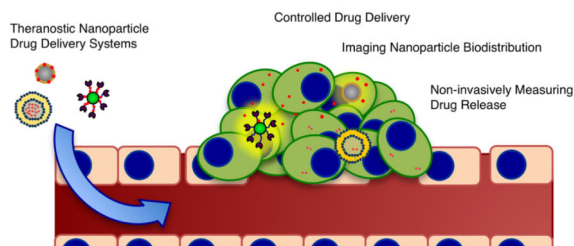
Thomas Moore[†], **Hongyu Chen**[‡], **Rachel Morrison**[†], **Fenglin Wang**[‡], **Jeffrey N. Anker**[‡,*], and **Frank Alexis**[†,*]

[†]Department of Bioengineering

[‡]Department of Chemistry, Clemson University, Clemson, South Carolina 29634, United States

Abstract

A wide variety of chemotherapy and radiotherapy agents are available for treating cancer, but a critical challenge is to deliver these agents locally to cancer cells and tumors while minimizing side effects from systemic delivery. Nanomedicine uses nanoparticles with diameters in the range of ~1–100 nm to encapsulate drugs and target them to tumors. The nanoparticle enhances local drug delivery effciency to the tumors via entrapment in leaky tumor vasculature, molecular targeting to cells expressing cancer biomarkers, and/or magnetic targeting. In addition, the localization can be enhanced using triggered release in tumors via chemical, thermal, or optical signals. In order to optimize these nanoparticle drug delivery strategies, it is important to be able to image where the nanoparticles distribute and how rapidly they release their drug payloads. This Review aims to evaluate the current state of nanotechnology platforms for cancer theranostics (*thera*peutic and diag*nostic* particles) that are capable of noninvasive measurement of release kinetics.

Keywords

theranostic nanomedicine; quantitative drug delivery; imaging delivery; cancer

*Corresponding Authors*janker@clemson.edu. falexis@clemson.edu..

INTRODUCTION

Today cancer persists as the second leading cause of death following cardiovascular disease in the United States.[1,2] While nanoparticle (NP) controlled drug delivery systems have significantly improved the clinical safety of chemotherapeutic drugs, effcacy of nanomedicines in the clinic has shown variable results.[3-5] For example, albumin-bound paclitaxel (Abraxane) has been shown to be significantly better than conventional paclitaxel when administered as a second line therapy.[6] Furthermore, a single agent clinical study for treatment of nonsmall cell lung cancer showed that Abraxane had clinical effcacy more similar to literature results for paclitaxel-carboplatin combination therapy.[3,7] BIND-014 is a prostate-specific membrane antigen-targeting polymeric PLGA-PEG NP loaded with docetaxel.[4] Preliminary clinical data showed disappearance or shrinkage of metastatic cholangio-carcinoma tumor lesions in the lungs of a 51-year old male patient after two treatment cycles with BIND-014 administered at 15 mg/m^2. Similarly, a 63-year old male with tonsillar cancer showed a 25% shrinkage in tumor lesions after two treatment cycles at 30 mg/m^2. These results are significant because docetaxel was administered via BIND-014 at doses lower than the typical dose for solvent based docetaxel (75 mg/m^2). Furthermore, docetaxel is expected to have minimal activity against cholangiocarcinoma, in the case of the 51-year old patient with lung metastases. On the contrary, some NP mediated drug delivery systems have shown variable improvements in treatment effcacy. Doxil, a liposomal form of doxorubicin, significantly decreased cardiac toxicity associated with the free drug. However, a phase III study of the clinical effcacy of Doxil compared to conventional doxorubicin showed that liposomal doxorubicin effcacy was comparable to, but not significantly better than, conventional doxorubicin.[8] Paclitaxel polyglumex, a macromolecule composed of paclitaxel conjugated to polyglutamic acid, also showed no significant improvement compared to docetaxel as a second line treatment to nonsmall cell lung cancer.[9,10] A number of other NPs such as CRLX101,[11] NK105,[12] Genexol-PM,[5,13] and BIND-014[4] have completed, or are enrolling, phase I/II/III clinical trials. The results of these studies are needed to further identify potential benefits or limitations of nanomedicines in clinical translation.

Significant challenges facing chemotherapy include rapid drug clearance, poor biodistribution, nonideal physicochemical properties of drugs (e.g., poor solubility), rapid drug degradation, and systemic toxicity.[14] Nanomedicine has been able to overcome some of these challenges. Preclinical data and phase I/pharmacokinetic clinical studies have shown that nanomedicines have been able to extend the circulation half-life of some chemotherapy drugs. For example, paclitaxel was shown to have a biphasic plasma elimination curve when administered with polyoxyethylated castor-oil, while Abraxane showed a linear curve.[15,16] NP formulations have also shown extended circulation time for chemotherapy drugs.[9,12,15-17] Nanomedicines may also take advantage of inherent physiological abnormalities in tumors such as the overexpression of certain proteins or leaky vasculature. These abnormalities allow NP drug delivery systems to increase intratumoral drug concentration via active targeting or the enhanced permeability and retention effect.[4,18,19] However, as previously discussed, NP drug delivery systems have shown variable clinical success. This is largely due to wide intratumoral and interpatient

heterogeneity.[20-22] Thus, a new paradigm is necessary to noninvasively determine the dose of drug delivered into the patient's tumor, and adjust further treatment.

Currently, treatment effcacy and disease progression are monitored via imaging (CT, MRI, ultrasound, X-ray, endos-copy/laparoscopy) and tumor markers in blood or in tumor tissue.[23,24] These indirect approaches are not able to provide immediate feedback as to how and where drug is released. Prolonging the local delivery of chemotherapeutic agents is expected to increase therapeutic effcacy against solid tumors, and a modality capable of monitoring drug biodistribution, intratumoral drug concentration, and therapeutic effcacy would provide critical information regarding treatment progress. Moreover, chemotherapy dosing is generally administered based on patient body surface area, and such a treatment modality would offer more personalized treatment plans that could account for patient heterogeneity, variation in diseases, variation in drug biodistribution, and differences in treatment response.[21,25] Herein we describe recent advances in nanoparticle systems capable of not only improving intratumoral drug delivery, but also noninvasively and quantitatively evaluating drug release kinetics in vivo.

THERANOSTIC NANOMEDICINE

Theranostic nanomedicines, systems that combine therapeutic and diagnostic modalities into a single package, are expected to provide real-time information of a drug delivery system's biodistribution, drug concentration, or drug release kinetics (Figure 1). The National Institute of Health (NIH) Challenge Grants in Health and Science Research, part of the American Recovery and Reinvestment Act of 2009, outlined the urgent goal of finding effective systemic treatments that can validate the localization of drug at the tumor site in real time, that is, smart, theranostic biomaterials.

The first generation of theranostic nanomedicines focused on combining both therapeutic and imaging modalities to image the localization of the drug delivery vehicle at the tumor. Much literature exists evaluating the current state of these combined imaging and delivery technologies.[21,26-32] These systems generally rely on NPs with discrete imaging and drug delivery components. In this approach, the imaging modality is independent of drug delivery. By combining drug delivery and imaging, theranostics enables visualization of drug biodistribution, and determination of the amount of nanoparticle drug delivery vehicle accumulated at the disease site.[21,28-31] First generation theranostic nanomedicines may be composed of a number of different types of NPs. Magnetic NPs are of considerable interest for theranostic applications due to their capacity for drug delivery, controlled localization in vivo,[33] and MRI contrast.[34,35] Moreover, magnetic NPs may be combined with other nanocarriers to impart optimal drug delivery properties.[36,37] Other systems capable of combined imaging and release include gold nanoparticles (AuNP),[38] carbon nanotubes (CNT),[39-42] quantum dots (QD),[43,44] polymeric NPs,[45-50] nanobubbles,[51] and liposomes.[26] While these technologies offer approaches to combine imaging and drug delivery, many lack the capacity to quantitatively measure drug release kinetics in real time.

The appeal of theranostic approaches that can quantitatively measure drug release kinetics exists, because such an approach would enable better understanding of intratumoral drug

concentrations. Considering that therapeutic agents are, in general, inactive until released from their respective nano-carriers, a theranostic modality capable of noninvasively quantifying drug release would also provide a better indication as to the dose delivered to a tumor by differentiating between encapsulated and released drug. Furthermore, research aimed at developing triggered release systems (i.e., light, pH, heat) is expected to benefit by enabling a noninvasive method for not only ensuring proper drug localization, but also determination of released drug concentration. Such systems would also benefit preclinical development of nanomedicines by improving means of optimizing release kinetics, especially in complex in vivo models. Traditional pharmacokinetics approaches such as quantification of radiolabeled drugs in tissue using positron emission tomography (PET), single photon emission tomography (SPECT), or radiology are valuable for measuring total drug accumulation rates in tissue. However, they cannot distinguish free drug that has been released from a NP from encapsulated drug. Consequently, a frontier of theranostics is to measure in situ release rates using imaging modalities that depend upon whether the drug is encapsulated or free. Below, we describe methods to detect drug release through tissue using MRI and optical techniques. Table 1 shows a summary of the technique's advantages and limitations.

OPTICAL APPROACHES TO MEASURING DRUG RELEASE

Theranostic nanotechnologies with the ability to quantitatively measure the release of drug would provide critical data regarding delivered drug dose in real time. Noninvasive optical methods are often used to monitor concentration of fluorescent drug in tumors.[52-56] In order to measure drug release rate independent of NP accumulation, the free drug must have a different spectral signature when released versus when encapsulated. The most common approach relies on fluorescence quenching of the drug when encapsulated in the NP due to self-quenching at high concentration or energy transfer to a quencher such as another dye or a gold NP. Release of the drug from the NP results in increased fluorescence intensity and lifetime of the drug. Other methods rely upon distance dependent inner filter absorption effects, changes in the local refractive index in photonic crystal structures, and methods to magnetically modulate the dye only when it is attached to the particle.[43,57-60] Optical techniques are widely used for measurements in cell studies and thin tissue histology because the microscopes are widely available and provide rapid, sensitive, submicrometer resolution images. However, imaging through thick tissue is more challenging because the light is attenuated as it passes through the tissue, autofluorescence backgrounds can obscure the analyte signal, and the diffuse scattering dramatically reduces image resolution.

Porous Silicon Photonic Crystals

Silicon is a biocompatible material that can be patterned with electrochemical and lithographic technique to generate very versatile drug carriers. For example, silicon can be electrochemically etched to generate nanopores that can be loaded with drugs. The width of the pores can be controlled during electrochemical etching to produce rugate structures with sharp spectral reflection features, similar to the photonic patterns in beetles and butterflies.[61] The reflection spectrum depends upon the refractive index of the medium in the pores and shifts as the drug is released from the pores. Porous silicon (PSi) microparticles have been

shown to quantitatively measure the release of the anticancer drug daunorubicin (Figure 2).[62] Plate-shaped microparticles approximately 12 μm by 35 μm were loaded with daunorubicin by covalently linking the drug to the microparticle surface via 1-undecylenic acid. Dissolution of the PSi microparticle resulted in zero-order release kinetics of daunorubicin and orthosilic acid. The colorimetric shift in λ_{max} could be directly correlated with the release of daunorubicin. To further verify that daunorubicin release was mediated by the dissolution of PSi microparticles, daunorubicin-conjugated microparticles were incubated in pH 5, 7, and 9. More alkaline pH catalyzed the dissolution of PSi, and daunorubicin release studies showed that increasing pH led to more rapid release of orthosilicate and daunorubicin. Increasing pH also led to more rapid spectral peak shift. Thus, porous PSi microparticles enable the quantitative measure of drug release.

PSi has also demonstrated inherent photoluminescent properties which may be amenable for in vivo imaging applications.[63-67] Porous silicon NPs approximately 126 nm in diameter and coated with dextran were able to load 4.4 wt % doxorubicin via the electrostatic interaction between drug and the porous silicon nanoparticles.[64] NPs mediated the release of doxorubicin over a 10 h period. Furthermore, PSi NPs were photoluminescent with an excitation wavelength in the ultraviolet region (370 nm) and emission maximum around 800 nm. PSi NPs were also biodegradable and dissolved within 8 h in phosphate buffered saline. As PSi NP degraded, their photoluminescent intensity not only decreased but also exhibited a blue shift of the luminescence spectrum. However, PSi NPs were not shown to enable quantitative imaging of doxorubicin release.

Thus, PSi particles are a platform for imaging drug release. While use of photoluminescence to image was not shown to quantitatively measure drug release from PSi NPs, spectral reflectance was shown to directly measure the release of daunorubicin from PSi microparticles.[62,64] However, imaging reflectance in vivo to measure drug release would be limited to relatively thin tissue depths or transparent tissues (e.g., intraocular drug delivery).

Fluorescent Drug Accumulation and Singlet Oxygen Luminescence

In some instances, the drug itself serves as the imaging and therapeutic agent. This can be attributed to inherent imaging properties of the drug. For instance, pH-sensitive NPs composed of poly(ethylene glycol)-*co*-poly(*β*-amino ester) (PEG-PBA) were shown to deliver the photosensitizer protoporphyrin IX (PpIX) for combined photodynamic therapy and imaging (Figure 3).[58] In this system, PEG acts as a NP-stabilizing corona and PBA loads the hydrophobic drug. PBA is protonated at its tertiary amine at lower pH, causing the polymeric micelle to destabilize and release its PpIX payload. Aside from being a photoactive drug, PpIX is also a fluorescent molecule and can therefore be used for imaging. The PpIX fluorescence is quenched by molecular oxygen, thereby generating singlet oxygen which is believed to be the primary effector responsible for killing cells. Three types of information are available: the PpIX can be localized based upon fluorescence microscopy and optical tomography, the local dissolved oxygen concentration can be measured based upon the fluorescence lifetime,[68] and the amount of singlet oxygen generated during photodynamic therapy can be measured by detecting the singlet oxygen luminescence at 1270 nm.[69,70] In vitro fluorescence measurements showed a pH-dependent release of PpIX

over a 72 h period with up to 60% of drug released within the first 24 h at pH 6.4. At physiological pH of 7.4, only 20% of drug was released after 72 h. Fluorescent imaging of SCC7 squamous cell carcinoma in vitro showed more uptake of PpIX at lower extracellular pH. This is ostensibly due to the destabilization of PBA-PEG micelles and release of the PpIX payload when internalized via lysosomes. Subcutaneous SCC7 tumor xenografts showed accumulation of PpIX-loaded PBA-PEG NPs in tumors. Five milligrams of PpIX per kilogram of mouse mass was injected via the tail vein as either free PpIX or PpIX encapsulated in PBA-PEG NPs. PpIX was imaged fluorescently using a 670 nm pulsed laser diode excitation source. Kinetic fluorescent biodistribution studies showed an increased accumulation of PpIX in tumor tissue over a 48 h period when delivered via the PBA-PEG nanoparticles, as opposed to free PpIX. The relative fluorescent intensity of PpIX was calculated as 10-fold higher in tumors when administered with PBA-PEG nanoparticles compared to free drug. Explanted tissues showed an appreciable accumulation of PpIX in the liver tissue for the free PpIX, while PpIX delivered via PBA-PEG showed strong fluorescent signal in the explanted tumor. This platform shows potential for the quantitative monitoring of drug delivery in vivo based on the fluorescent properties of the drug molecule. This system was shown to be effective in SCC7 squamous cell carcinoma in superficial, subcutaneous tumor grafts. However, feasibility of this therapy in a deeper tissue was not explored and is likely to be limited because the 670 nm excitation wavelength is attenuated by a factor of between 10 and 1000 per centimeter of tissue depth, depending on the type of tissue.[71] Treatment of tumor 1 cm and deeper would therefore require either an endoscopic light source or a method to apply light over a period of days.

Fluorescent Nanoparticles

A different approach to employing fluorescence as a theranostic modality is to utilize fluorescent NPs. A QD drug delivery system was reported in which fluorescence resonance energy transfer (FRET) allows for fluorescent imaging of both NPs and delivery of drug.[43] Dox was employed as the drug model due to its inherent fluorescence (Figure 4). Here, the QDs are functionalized with a double-stranded A10 RNA aptamer that intercalates Dox and specifically binds prostate specific membrane antigen (PSMA). The QD–aptamer–Dox construct (QD-Apt(Dox)) is "turned off" because Dox quenches the fluorescent emission of the QD, and the aptamer quenches the fluorescent emission of Dox. Upon the release of Dox, both entities become fluorescent, allowing for the visualization of both NP and drug location. PSMA is overexpressed in LNCaP human prostate cancer cells but not PC3 human prostate cancer cells; therefore, LNCaP cells were qualitatively shown to uptake more QD-aptamer (QD-Apt) conjugates than PC3 cells in vitro. After incubating LNCaP cells for 30 min with QD-Apt(Dox), cells were washed and imaged with confocal microscopy. At this time, cells showed no fluorescence, indicating a lack of drug release. However, after incubating for 1.5 h, more fluorescent signal could be seen in the cell from both Dox and QD. Thus, the QD-Apt(Dox) conjugate could be used to image the release of drug in vitro. Moreover, QD-Apt were sensitive to the quantity of Dox loaded. QD-Apt held at a fixed concentration (1 μM) were incubated with increasing amounts of Dox, and maximum FRET quenching was observed at a QD-Apt/Dox ratio of 1:7. As a chemotherapeutic agent, QD-Apt(Dox) conjugates at 1.6 μM were approximately as effective as free Dox at 5 μM. A similar system was employed to improve the delivery of free Dox to A2780/AD multidrug

resistant human ovarian cancer in vitro and in female athymic nu/nu mice.[72] QDs were conjugated to an aptamer (MUC1) which targets mutated Mucin 1, a cell surface-associated mucin overexpressed in late stage epithelial ovarian cancer. Dox was conjugated via an acid-degradable hydrazone bond. Similar to the Bagalkot study, QD-MUC1(Dox) conjugates displayed FRET extinction of QD fluorescence. Free Dox, QD-Dox, and QD-MUC1(Dox) showed similar treatment effcacy in vitro. In vivo, targeted QD-MUC1 showed higher uptake compared to untargeted QD. No tumor volume reduction data was reported for in vivo effcacy. The primary utility of these two systems from a theranostic drug delivery system standpoint is as an "on/off" switch indicating drug loaded or released. Compared to polymeric systems in which drug is encapsulated, these systems load much lower amounts of drug and have relatively quick release. One limitation related to in vivo imaging is associated with poor penetration of excitation wavelengths through tissue. Although this system is unable to measure the release kinetics based on FRET extinction, other systems capable of dynamically measuring release rates have been developed.

Rare earth-doped nanophosphors are a class of inorganic materials that are able to convert various forms of electro-magnetic radiation into visible light. Different classes of nanophosphors can convert ultraviolet light (fluorescent phosphors), infrared light (upconversion phosphors), or X-ray (radioluminescent phosphors) into visible light. Nano-phosphors are advantageous compared with organic dyes because these rare earth-doped inorganic phosphors have a high chemical stability and do not photobleach or fade.[73,74] Nanophosphors also have distinct spectral peaks with narrow fine structure (~1 nm line-width) compared to 20–100 nm line width for quantum dots and fluorescent molecules,[75] and their low toxicity draws attention to their biological applications.[34,75,76] NPs with short ultraviolet (256 nm) excitation wavelength and emission of visible light (613 nm) were employed to measure drug loading and release.[77] NPs were composed of a spherical europium-doped gadolinium oxide core (Gd_2O_3:Eu^{3+}) approximately 270 nm within a mesoporous silica ($@nSiO_2@mSiO_2$) shell approximately 50 nm thick. Dox is able to load at 8.56 wt % within the pores of the mesoporous silica and quench the luminescent emission signal of the Gd_2O_3:Eu^{3+}. Release studies revealed that Gd_2O_3:Eu^{3+} $@nSiO_2@mSiO_2$ NPs released 80% of loaded Dox over approximately 12 h. The photoluminescence of the Gd_2O_3:Eu^{3+} was measured as Dox was released. These simultaneous studies of NP luminescence and Dox release showed a direct relationship between the amount of Dox released and increasing NP photoluminescent intensity. These results indicate that the Gd_2O_3:Eu^{3+} quenching effect of Dox is mitigated as it is released from the mesoporous silica shell, and photoluminescence returns. In vitro studies of Gd_2O_3:Eu^{3+} $@nSiO_2@mSiO_2$ NPs in HeLa cervical cancer cells showed no concentration dependent toxicity up to 2.5 μg/mL. Free Dox and Dox-loaded NPs showed equivalent effcacy in vitro against HeLa cells. This system is limited for translation to in vivo diagnostics because the UV excitation wavelengths are strongly absorbed by melanin in skin.[78-80] Furthermore, high energy UV radiation has deleterious effects on DNA and may lead to protein–DNA cross-linking, oxidative damage, and gene mutations.[81]

Upconversion Nanoparticles

Visible and UV light phosphors are expected to have limited application for deep tissue imaging due to light scattering and the poor penetration depth of shorter excitation wavelengths.[82] Recent research is focused on upconversion NPs, particles that can convert longer near-infrared (NIR) wavelength light to visible light (Figure 5). Upconversion probes capable of excitation at longer wave-lengths and emission within the optical transmission window (650–950 nm) are promising due to low tissue autofluorescence, deeper tissue penetration of excitation wavelengths, and lower light scattering. It has been shown that upconversion particles can image as deep as 3.2 cm through pork tissue with excitation at 980 nm and emission at 800 nm.[83] Upconversion NPs have been investigated as a means to track drug release by measuring luminescent intensity.[84,85]

Theranostic upconversion NPs composed of sodium yttrium fluoride ($NaYF_4$) doped with ytterbium and erbium (Yb^{3+}, Er^{3+}) have also been described.[85] Similar to the previously mentioned Gd_2O_2:Eu^{3+} NPs, the $NaYF_4$:Yb^{3+}/Er^{3+} were coated with mesoporous silica (@$nSiO_2$@$mSiO_2$). In this system ibuprofen (IBU) was chosen as a model drug and loaded into mesoporous silica. The $NaYF_4$:Yb^{3+}/Er^{3+} core was 120 nm in diameter and coated with a tunable level of mesoporous silica (10, 20, or 45 nm). These NPs were capable of loading 11, 21, or 34 wt % IBU in the 10, 20, or 45 nm mesoporous silica coatings, respectively. All three formulations demonstrated controlled release over a 10 h period, with changes in release kinetics altered by coating thickness. Thicker coatings were hypothesized to slow release time due to the IBU having to travel farther through the mesoporous silica pores. IBU also effectively quenched the photoluminescence from the upconversion $NaYF_4$:Yb^{3+}/Er^{3+} @$nSiO_2$@$mSiO_2$ nanoparticles. NPs were excited by 980 nm wavelength light and had three emission peaks at 520, 550, and 650 nm. Release kinetics were directly correlated to the return of photoluminescence, indicating that as IBU was released, the quenching effect of IBU diminished. This system demonstrates a mechanism by which the release of drug can be dynamically measured due to the quenching of NP luminescence by the drug. This system successfully shows a robust method for quantitatively measuring drug release based on the upconversion luminescence of NPs. However, as with most inorganic delivery systems, the release kinetics are not optimized for controlled release. With the thickest mesoporous silica coating, 75% of IBU was released within 12 h. Upconversion NPs are expected to overcome some of the challenges for in vivo imaging associated with fluorescent molecules or NPs, but will still be limited in the penetration depth of the excitation and emission wavelength. Methods to improve drug loading and release kinetics have been investigated using organic coatings on inorganic NPs.

Upconversion NPs have also been coated with organic layers to improve lipophilic drug loading and aqueous dispersion.[59] In this study, cubic 20–30 nm $NaYF_4$:Yb^{3+}/Er^{3+} NPs were capped with oleic acid and further functionalized with *a*-cyclodextrin (*a*CD). Oleic acid was able to load lipophilic photosensitizers such as Chlorin e6 (Ce6), Zinc phthalocyanine (ZnPc) and Methylene blue (MB). *a*-Cyclodextrin improves the aqueous solubility of this system, and cyclodextrin has been used in clinical trials as part of a NP drug delivery system.[48,49] In this system, the upconversion particles were excited by a 980 nm laser, then they emitted strongly in the 650–670 nm range. Ce6, ZnPc, and MB had

strong absorptions in this region. Loading capacity for all three photosensitizers was dependent on the loading photosensitizer concentration, and total loading between drugs was variable, possibly due to differences in chemical structure. Ce6, ZnP, and MB were able to load at 0.158, 0.165, and 0.129 mmol/g, respectively. Luminescent intensity of the NPs was quenched by loading the photosensitive drug, and the release of photosensitizer allowed for a dynamic method to measure drug release. Release studies showed that approximately 10% of drug was released in 48 h.

In vitro toxicity of photosensitizer-loaded upconversion NPs was shown in A-549 adenocarcinomic human alveolar basal epithelial cells. Photosensitizer-loaded NPs without laser irradiation showed no significant toxicity in cells. When irradiated with the 980 nm laser (1 W/cm^2) for 3 min, upconversion luminescence activates the photosensitive drug, creating reactive oxygen species. The irradiated NP showed dose-dependent toxicity in vitro, and toxicity was also dependent on the duration of laser irradiation. This photodynamic therapy was combined with traditional chemotherapy by loading Dox in the NP. The combination of Dox and photodynamic therapy significantly improved therapeutic effcacy of the NP. For example, NPs loaded with 0.077 mmol/g Ce6 and 0.082 mmol/g Dox irradiated with 980 nm laser showed approximately 15% cell viability with A-549 cells in vitro. This was significantly better than NPs loaded with Ce6 and Dox without irradiation (~40% cell viability) or Ce6 NPs with irradiation (~40% cell viability). While these treatments are effective in vitro, near-infrared and infrared wavelengths are still limited in translation to deep tissue imaging because the penetration depth is on the scale of millimeters.[82] Technologies with greater potential to penetrate deep into tissue are expected to improve theranostic modalities.

Radioluminescent Nanoparticles

Radioluminescence is a phenomenon whereby radiation energy is converted into visible light, and here we will focus upon X-ray radiation although some of the principles also apply to other forms of radiation. The benefit of using this type of system for measuring drug release is that X-ray has excellent soft tissue penetration. Radioluminescent nanophosphors have been investigated for in vivo imaging and as quantitative sensors for drug delivery.[57,83,86] Theranostic radioluminescent NPs coated with poly(styrenesulfonate sodium) (PSS) and poly(allyl-amine HCl) (PAH) via a layer-by-layer assembly were designed for pH-sensitive drug release.[57] The hollow NP was composed of gadolinium oxysulfide (Gd$_2$O$_2$S) doped with terbium (Tb) and europium (Eu) (Figure 6). NPs were ellipsoidal in shape with an average length of 420 nm and a width of 150 nm. Higher aspect ratio NPs have been shown previously to extend plasma circulation time in vivo.[87-89] The Gd$_2$O$_2$S:Tb-PSS/PAH NPs were able to load ~5 wt % Dox, and release measured by high performance liquid chromatography directly correlated with peak quenching of the NP radioluminescence. Moreover, Dox release was shown to be pH dependent with rapid release at pH 5.0 and slow release at pH 7.4. The goal of pH dependent release is to exploit intracellular release of drug in endosomes or lysosomes after endocytosis. NP uptake was shown in MCF-7 breast cancer cells, and in vivo biodistribution showed the ability to dynamically and noninvasively monitor radio-luminescent NP accumulation in the liver of Balb/c mice. Previous studies have shown the ability of radioluminescent NPs for deep

tissue imaging in chicken breast after injection deeper than 1 cm.[83] This system offers a promising platform for theranostic nanomedicine due to excellent penetration depth of X-rays through soft tissue.

A key advantage of this approach is that there is almost no autofluorescence background, and the radioluminescence is only generated where the X-ray beam irradiates the tissue. By irradiating the tissue with a collimated or focused X-ray beam, it is possible to map the spectrum point-by-point in order to generate high resolution images, limited in resolution by the X-ray beam width. This is in contrast to fluorescence excitation, wherein the excitation beam is scattered with a typical mean free path of ~100 μm, and almost all the light passing through more than 1 mm of tissue propagates diffusively providing a point spread function with a width similar to the tissue depth.[90,91]

The main limitation of the X-ray excited optical luminescence imaging is that radioluminescent systems may be limited by the penetration depth of visible light emissions, even though X-rays have excellent soft tissue penetration. In general, there is a trade-off between the required X-ray dose and the scintillator concentration, the depth of the scintillators in the tissue, and the spatial resolution of the image. For example, in a numerical simulation, Carpenter and co-workers calculate picomolar (ng/mL) concentrations of 10 nm X-ray phosphor are detectable for a mammographic-like dose with a signal/noise level of 10.[92] For applications such as tumor resection where the X-ray excitation angle is limited by geometry, and where increased rapid acquisition is critical, a limited-angle X-ray luminescence tomography (XLCT) can be applied based on a hybrid X-ray/optical reconstruction. In XLCT X-rays, pencil-like X-rays are used to excite scintillators in a narrow region defined by the beam diameter, and diffuse optical spatial discrimination for the axial dimension along the beam. According to their model, microgram per milliliter particle concentrations may be observed through 5 cm of tissue with ~10 mGy doses.[93] Even more rapid images can be acquired using a cone-angle geometry with multiple angle views, but the resolution will be limited by the optical scattering in the tissue.[94]

Nanophosphors (luminescent nanoparticles) exist as a potential platform for a theranostic system able to quantitatively measuring drug delivery at the bench. These NPs can be tailored to have excitation wavelengths over a broad range, from X-ray to near-infrared light. Employing NPs with luminescence that overlaps with the optical properties of drugs has been shown to quantitatively measure the release of drug. The use of these NPs in a clinical sense is still limited by specific challenges, namely, nanoparticle-associated toxicity and physical limitations. Currently, optical imaging in tissue is limited to the millimeter or centimeter depth. Thus, identifying and addressing current imaging challenges will guide decisions for future research.

MAGNETIC RESONANCE IMAGING (MRI) OF DRUG RELEASE

Magnetic resonance imaging (MRI) is particularly attractive as a theranostic imaging modality. MRI is not limited by imaging depth, and can also be used to quantitatively measure drug release. MRI works via the magnetization of hydrogen protons, generally from water, in tissue. Briefly, a strong magnetic field is applied to the patient, causing protons to

align in the direction of the magnetic field, and a short electromagnetic pulse causes the perturbations to the proton's spin. Protons release energy as they return to alignment, and two measurements can be made: return to longitudinal magnetization (T_1 relaxation), or decay of transverse magnetization (T_2 relaxation).[95,96] Since tissues are different structurally, they will appear differently on an MRI image. In cancer imaging, magnetic NPs localized at the tumor site may enhance the contrast of cancerous lesions by altering the spin relaxation of neighboring water molecules.[97]

Generally, theranostic MRI approaches have relied on drugs that are complexed with an imaging agent, or drugs that can release at the same rate as an imaging agent. Externally triggered drug release systems are therefore appealing, because simultaneous triggered release of an imaging agent and drug is possible. The use of hyperthermia to control both the timing and spatial location of drug release, via hyperthermia or some other modality, was termed "dose painting."[98] In the following approaches, MRI enables a means to noninvasively determine drug dose and spatial location of release, giving a more clear understanding of how drug is distributed within the tumor.

Theranostic MRI was enabled via liposomes that encapsulated two components: doxorubicin (Dox), an anthracycline anticancer drug, and manganese sulfate, an MRI contrast agent.[60,98-100] Temperature sensitive liposomes less than 200 nm in diameter were prepared to destabilize and release drug at hyperthermic temperatures (39 to 40 °C).[101] In this study, Dox molecules complex with manganese ions (Mn^{2+}), and these ions are able to act as T_1-shortening MRI contrast agents. Within the liposome, MRI contrast is diminished because T_1-shortening is dependent upon interaction of water with the Mn^{2+}, and sequestration of Dox-Mn^{2+} within the liposomes reduces the interaction of Mn^{2+} with water. The MRI contrast is only actuated when the Dox-Mn^{2+} complexes are released from the liposome (Figure 7).

Rats were implanted subcutaneously with rat fibrosarcoma tumors, and liposomal treatments were administered intra-venously.[60] Treatment groups included local hyperthermia (HT) + temperature-sensitive liposomes (TSL), no hyper-thermia (nHT) + TSL, HT + nontemperature-sensitive liposome (nTSL), and nHT + nTSL. T_1-weighted MRI images were compared to HPLC analysis, and fluorescent histological analysis of explanted tumor tissues after treatment with liposomes. HPLC data showed a strong correlation in drug concentration with image analysis of MRI contrast agents in tissue, indicating that MRI was a sensitive, noninvasive modality to measure the hyperthermia-mediated release of Dox in vivo. This approach was able to measure Dox release in vivo at μg/mL concentrations. This approach has the benefit of being able to quantify drug release in deep tissue. Further studies on the influence of hyperthermia treatment with TSL dosing showed that the highest amount of Dox was delivered to tumors when TSL were administered during HT.[98] Rats that received TSL before HT had a final mean Dox accumulation in tumors of 24.5 μg. A split-dose regimen was administered by injecting half of the TSL dose prior to HT, and the second half after the HT treated tumor had reached a steady state temperature. This split-dose treatment regimen resulted in a final mean Dox accumulation of 33.5 μg. Finally, administration of TSL during HT resulted in the highest mean Dox accumulation of 39.5 μg. HT treatment regime also played a role in determining the spatial distribution of Dox release

within the tumor. Dox dose location was measured via MRI. The source of heating was an intratumoral catheter, thus administration of TSL during HT resulted in rapid release of Dox at the periphery of the tumor. This is caused by the quick destabilization the TSL upon reaching the preheated tumor. Administration of TSL in the split-dose treatment regimen resulted in the most uniform distribution of Dox throughout the tumor, and administration of TSL before HT treatment resulted in rapid release in the center of the tumor (near the HT catheter). Tumor reduction studies showed that TSL administration during HT had the most significant effect. Tumor inhibition was measured in time needed to reach a tumor volume five times greater than the initial tumor volume. TSL administration during HT had a mean time of 34 days, the split-dose regimen had a mean time of 22.5 days, and TSL administration before HT had a mean time of 18.5 days. TSL administration during HT was not significantly different than the split-dose treatment.

Because some research has raised questions about the cytotoxicity of manganese ions, work has pushed for a gadolinium-based theranostic system.[102,103] Gadolinium is in clinically approved MRI contrast agents at concentrations as low as 0.1 mmol/kg body mass, and several researchers have reported temperature sensitive liposomal formulations coencapsulated Dox and gadolinium-based MRI contrast agents.[104-108] For example, MRI quantification was possible by measuring the corelease of Dox and gadolinium-diethylene triamine pentaacetic acid complex (Gd-DTPA) (Figure 8).[104] Here Gd-DTPA is not complexed with Dox, rather Gd-DTPA models the release of Dox. Gd-DTPA showed similar release kinetics to Dox in vitro. At 30 and 37 °C, there was no detectable release of Gd-DTPA over 30 min, while at 40 and 42 °C there was total Gd-DTPA release within 3 min. Dox release showed similar results where 100% Dox was released within 3 min at 40 and 42 °C. Fluorescent readings of explanted tumor tissue showed a strong correlation between Dox in tissue and Gd-DTPA content measured via MRI. Furthermore, liposomal formulations combined with hyperthermia-mediated Dox release were able show a dose-dependent inhibition of tumor growth in vivo.

While the previous temperature sensitive liposomal treatments employed either invasive or indirect means for heating tumors, and consequently releasing TSL payloads, some researchers noninvasively induced drug release via magnetic resonance-guided high intensity focused ultrasound (MR-HIFU).[105,106,108] TSL were coloaded with Dox and Gd-HP-DO3A, an FDA-approved gadolinium-based MRI contrast agent. Dox and Gd-HP-DO3A release were measured via fluorescence and inductively coupled plasma-atomic emission spectroscopy, respectively. Differences in release profiles between these two agents were shown to be less than 20%.[108] MR-HIFU was also shown to enable a high degree of control over the location of heating. Tissues mimicking agarsilica phantoms were cast containing TSL. MR-HIFU was used to heat distinct geometric patterns in the gel, which resulted in visualizing these distinct shapes. Furthermore, MR-HIFU induced the release of Gd-HP-DO3A in vivo with New Zealand white rabbits bearing VX2 tumors in the thigh. Focused ultrasound was able to generate a local temperature increase at the site of the tumor, and result in an increase in MRI contrast due to the release of Gd-HP-DO3A from TSL. Researchers were able to load Dox at clinically relevant concentrations (~25 mg/m2) while also delivering Gd-HP-DO3A at a concentration that could effectively enhance MRI contrast.

Similarly, researchers showed that MR-HIFU enabled visualization of drug release from TSL in vivo with 9L gliosarcoma tumor-bearing Fisher 344 rats.[105,106] MR-HIFU was able to induce the release of Dox and Gd-HP-DO3A in tumors. However, researchers did find widespread intersubject variability, which was attributed to differences in tumor vascularization, tumor permeability, as well as the presence of a necrotic core. Importantly, the authors note that in a complex biological environment the differences in cellular uptake and intratumoral distribution of Dox and the contrast agent will be significant upon release from the TSL. Thus, while a strong correlation was shown between Gd and Dox content in tumors, more robust pharmacokinetic modeling of drug versus contrast agent behavior is needed to better understand how these TSL may be employed in a clinically relevant manner to measure drug content in vivo.

A nonliposomal approach was to encapsulate Gd-DTPA within a poly(acrylic acid)-coated iron oxide NP (IO-PAA) (Figure 9).[109] Release was pH dependent due to the swelling and degradation of PAA in an acidic medium. In this system, the iron oxide core affects Gd-DTPA encapsulated within the PAA coating, effectively "quenching" the T_1 relaxation rate Gd-DTPA. However, as Gd-DTPA is released, the T_1 relaxation rate increases. Thus, encapsulated Gd-DTPA was "off," while released Gd-DTPA was "on." In addition, the particle concentration could be determined from the T2 contrast, which depends mostly on the iron oxide core rather than the Gd-DTPA. When Gd-DTPA was coencapsulated with another drug within the IO-PAA, it was possible to roughly approximate the release kinetics of both agents based on the T_1 relaxation of Gd-DTPA as it is released. Paclitaxel (PTX) and Gd-DTPA were loaded within IO-PAA. Release kinetics for PTX and T_1 relaxation were measured at pH 7.4 and 5.0 over a 24 h period. At pH 5.0, both agents were totally released after 24 h. Release of Gd-DTPA was slower than release of PTX, and the difference in release was attributed to physicochemical interaction between the Gd-DTPA molecules and the polymer coating.

These studies illustrate methods by which drug release kinetics could be measured by the release of an imaging agent–drug complex, or by measuring the corelease of separate drug and imaging agents. Moreover, release could be triggered due to physiological changes (e.g., differences in pH), or through external stimuli such as temperature. MRI was effective for imaging drug release at better than millimeter resolution through thick tissue. However limitations include cost, possible differences in release rates for drugs and imaging agents when coencapsulated, and different pharmacokinetic and pharmacodynamic behavior between released drug and imaging agent.

CHALLENGES IN THERANOSTIC NANOMEDICINE

Real challenges exist with the development of theranostic nanomedicines to enable noninvasive measurement of drug delivery. Nanomedicines must demonstrate reasonable safety. Many particles used for imaging have shown success in vitro for cellular labeling but are limited in translation to more complex living systems due to toxicity. Furthermore, theranostic particles must overcome physical limitations with respect to penetration depth of light due to scattering, and developing sensitive methods to image drug or NP.

Preclinical Challenges

A fundamental understanding of nanomaterials is necessary to develop practical theranostic technologies. This includes an understanding of material choice, limitations and advantages due to physicochemical properties, and potential nanomaterial related toxicities. Hesitance to employ nanomaterials for medical applications often stems from concerns regarding nanomaterial toxicity. Although NP toxicity is an important concern, several NP formulations have reached clinical trials. NP toxicity may generally be attributed to nanoparticle's material, degradation, size, shape, and in vivo stability.

One of the primary challenges surrounding the use of NPs for in vivo imaging and diagnostics pertains to the materials selected for use. For example, quantum dots (QD) have garnered much excitement for use as in vitro fluorescent tags; however, concerns about their toxicity arise because QDs are generally made out of heavy metal elements such as cadmium selenium (CdSe), cadmium tellurium (CdTe), and zinc selenium (ZnSe).[110] Generally QDs have a core–shell structure to reduce cytotoxicity, but studies have shown that QD toxicity is still related to heavy metal ions.[111] CdSe QDs oxidized in air or with UV light showed a red shift in fluorescence, indicating a change in size because of the leaching of surface atoms due to oxidation. QDs kept in an inert environment, that is, no oxidation, showed no toxicity in vitro against primary rat hepatocytes. However, when oxidized in air for 30 min, cell viability decreased to 21% at a QD concentration of 62.5 μg/mL. Free Cd^{2+} concentrations were determined from oxidized QD samples via inductively coupled plasma optical emission spectroscopy. QD oxidation in air resulted in a 21-fold increase in Cd^{2+} concentration, from 6 to 126 ppm. Thus, QDs generally require coatings, such as ZnS, to prevent leaching of toxic heavy metals. In a recent study, primates (rhesus macaques) injected with 25 mg/kg of phospholipid micelleencapsulated CdSe/CdS/ZnS QDs showed no evidence of toxicity over a period of 90 days. However, longer term studies will be needed to evaluate long-term effects, because the initial cadmium dose was cleared slowly from the liver, spleen, and kidneys.[112,113] More recently, Pluronic-encapsulated silicon quantum dots also showed no toxicity for 90 days in rhesus macaques in doses up to at least 200 mg/kg.[114]

Some nanomaterials have a historic track record for biocompatibility and have entered clinical trials. Gold, for example, has long been used as a biomaterial because it is relatively bioinert and stable.[115] Gold nanoparticles (AuNPs) have been employed as a therapeutic since the 1930s as treatment for rheumatoid arthritis.[116,117] Magnetic iron oxide NPs (IONPs) have also shown promise as nontoxic nanomaterials. While in vitro studies with RAW 264.7 rat macrophages indicated that 9 nm IONPs induced oxidative stress, cell viability and growth was not hindered.[118] Thus, nanomaterial stability in vivo seems to be key to determining a material's toxicity. AuNPs are considered bioinert and relatively nontoxic. QDs, however, have been shown to leach toxic metal ions, leading to cytotoxicity. Thus, the stability and degradability of a nanomaterials will be pertinent to prevented unintended toxicity.

NP size and shape also determine toxic response. Altering NP size and shape has been shown to greatly influence circulation time, biodistribution, toxicity, and cellular uptake.[87,88,119,120] Carbon nanotubes (CNTs) are a prime example of nanomaterials in

which toxicity is closely related to size and morphology. Several studies indicate that carbon nanotubes are safe when injected intravenously, and it appears that toxicity, fibrosis, and chronic inflammatory response are closely tied to the size and morphology, route of administration, dose, and surface functionalization.[121-127] Carbon-based nanomaterials such as carbon nanocapsules (CNCs), C_{60} fullerene (C_{60}), multiwalled carbon nanotubes (MWCNTs), and single-walled carbon nanotubes (SWCNTs) reportedly had different toxicity profiles due to differences in size and shape.[128] Carbon nanomaterials were dispersed in 1 wt % polyvinyl alcohol (PVA) and administered via tail vein injection. In both MWCNTs and SWCNTs, no mice survived after receiving 50 μg/g; however, 50% of mice receiving C_{60} and 91.7% of mice receiving CNCs survived at this dose.

Gold nanoparticles, on the other hand, show little toxicity associated with size and shape. In vitro studies with 4, 12, and 18 nm diameter NPs tested against K562 leukemia cells showed no toxicity up to 250 uM concentration.[129] Moreover, shape does not seem to play as large a role in AuNP-mediated toxicity. PEGylated gold nanorods approximately 65 nm long and 11 nm in diameter were injected at a concentration of 0.9 mM Au atom into male ddY mice, and at various time points mice were euthanized and organs were collected.[130] Gold content was quantified via ICP mass spectrometry, and gold nanorods had a circulation half-life of approximately 1 h, and were found up to 24 h in the blood. At 72 h, nanorods were absent from blood and 35% of initial injected dose had accumulated in the liver. In summary, nanoparticle-mediated toxicity appears to vary significantly between nanomaterial, size, shape, aggregation, and degradability. Thus, robust preclinical testing of nanomaterial safety and effcacy is required. However, aside from these fundamental materials challenges that exist, there are also clinical challenges in the translation of theranostic nanomedicines from bench to bedside.

Clinical Challenges

The previously described theranostic approaches are limited by drug modification, interaction of NPs and drugs, and optical imaging capabilities in deep tissue. With optical techniques in tissue imaging, viable wavelengths are generally restricted to the "biological window," a range of wavelengths from 650 to 1400 nm; we will refer to the spectral region from 650 to 1000 nm as the first optical window, and the region from 1000 to 1400 nm as the second optical window.[42,82,131-134] Wavelengths < 650 nm are strongly absorbed by hemoglobin, and those >950 nm light begin to be absorbed by water.[131,135] In addition to probe brightness and tissue penetration depth, optical signal must be larger compared to the background, especially if the background is large and variable. Reflected light spectroscopy (e.g., for the porous silicon rugate sensors) is thus especially challenging because of the large and variable background generated from the skin, although studies have succeeded in measuring the spectrum through at least 1 mm of human hand tissue because the peaks are narrow and distinct.[136] Fluorescent probes have far less background than reflection probes. However, autofluorescence background remains a problem, especially for low concentrations of dyes deep in tissue, and/or dyes with low quantum yields and absorption cross sections.[82] Imaging in the second optical window has shown promise with low incidence of autofluorescence and less tissue scattering. Single-walled carbon nanotubes are capable of sensitive in vivo imaging in the second optical window, and QDs which emit

within the second optical window showed significant improvement compared to imaging in the first optical window.[41,42,134] Alternatively, upconversion NPs for deep tissue imaging have been developed which are capable of imaging as deep as 3.2 cm through tissue.[83] However, approaches to image drug release in the biological window must rely on drugs and NPs that are either photoactive or absorb within this range of wavelengths. In the previously stated examples of NP systems that measure drug release based upon fluorescent resonance energy transfer, the NPs must be excited by a light which can penetrate deep into tissue. The drug must also be such that its absorption profile overlaps with the nanoparticle's emission wavelength within this window. To get meaningful data from a complex and dynamic in vivo system, the emitted light must overcome tissue scattering and be detected with enough sensitivity to measure drug release. The power of the excitation wavelength source and its distance to the NPs, the spatial distribution of the NP drug delivery system within the patient, and the sensitivity of the luminescent detection will complicate detection sensitivity in a deep tissue living system. Thus, while imaging limitations pose significant challenges to an optical theranostic approach, they also have important applications, including the clinical use of photosensitizers in photodynamic therapy.[137]

Phase I/II clinical studies are also required to validate the correct dosage, safety, pharmacokinetics, and biodistribution of nanomedicines. Since nanotechnology is relatively "new," less is known about long-term toxicity or complications compared to more conventional therapeutics. Nanomedicines may also vary significantly due to differences in manufacturing, and behavior may vary due to differences in physicochemical properties.[138] Nevertheless, companies have begun to enter the field in order to determine the feasibility of nanomedicines. Ensyce Biosciences, Inc. is currently researching carbon nanotubes as means for cancer therapy. While carbon nanotubes have traditionally been viewed as controversial biomaterial, mounting evidence suggests that appropriate surface coatings may mitigate toxicity associated with carbon nanomaterials.[139] Nanospectra Biosciences, Inc. has developed gold nanoshells meant to mediate hyperthermia, and has begun clinical trials of AuNPs for thermal ablation of solid tumors.[140-142] Tumor necrosis factor α (TNFα)-bound AuNPs functionalized with PEG have also been clinically tested and showed no adverse events in human clinical trials with concentrations from 50 to 600 μg/m2.[143] Finally, clinical trials for superparamagnetic and ultrasmall IONPs exist. The Food and Drug Administration (FDA) has approved Ferumoxtran-10 (AMAG Pharmaceuticals), a formulation of monodispersed 5–10 nm IONPs with a ~15 nm coating of dextran, for MRI contrast. Phase II clinical studies of intravenously administered Ferumoxtran-10 showed no significant events with doses up to 1.7 mg Fe/kg.[144,145] These are a handful of companies which have developed inorganic nanomaterials therapies aimed at translational, intravenous clinical use.

Noninvasively determining drug concentrations is becoming possible through increasingly sensitive imaging techniques.[146] Preclinical studies with the cyclodextrin polymer based nanoparticle (CRLX101) with polymer-conjugated camptothecin showed that biodistribution could be monitored using ^{64}Cu-labeled polymer.[49] While CRLX101 has advanced to early clinical trials, no efforts to pursue the positron emission tomography (PET) imaging aspect for a theranostic drug delivery approach have been reported. Use of PET is also limited due

to cost and the short half-lives of radioisotopes: from 2 min with ^{15}O to 109.8 min with ^{18}F.[147,148] Positron emitters with longer half-lives (e.g., 8.3 h for ^{52}Fe and 4.2 days for ^{124}I) are less commonly used because these elements are not found in many drugs and require a higher energy synchrotron to produce. Ideally, a theranostic nanomedicine to measure drug release will avoid modification of the drug, as this may affect release kinetics, biodistribution, and activity. Measuring the release of drug using MRI required complexing Dox with manganese ions, and the study employing modified gadolinium only modeled the release of Dox but did not measure its release from liposomes directly.[60,107] However, Dox/Gd-HP-DO3A TSL were loaded with clinically relevant concentrations of both Dox and the Gd-HP-DO3A imaging agent.[108] Thus, finding new ways to noninvasively measure drug release will need to not only overcome the latent challenges of nanomedicine (i.e., nanomaterial toxicity), and must also overcome translational issues such as imaging sensitivity.

CONCLUSION

Theranostic nanoparticles for noninvasive measurement of in situ drug release are being realized in laboratory studies. Current approaches are able to utilize drugs complexed with MRI contrast agents or take advantage of optical properties of drugs to measure drug release noninvasively. Nanotechnologies offer a platform to realize noninvasive measurement of drug concentrations, improve drug delivery and imaging of solid tumors, and improve drug biodistribution and effcacy. However, significant challenges in theranostic nanomedicine must be overcome, namely, the physical limitations of optical methods, complexities in imaging sensitivity and resolution in deep tissue, and toxicity of nanomaterials.

Acknowledgments

REFERENCES

(1). Howlader, N.; Noone, AM.; Krapcho, M.; Neyman, N.; Aminou, R.; Altekruse, SF.; Kosary, CL.; Ruhl, J.; Tatalovich, Z.; Mariotto, A.; Eisner, MP.; Lewis, DR.; Chen, HS.; Feuer, EJ. SEER Cancer Statistics Review, 1975-2009. National Cancer Institute; Bethesda, MD: 2011.

(2). Society, AC. Cancer Facts & Figures. American Cancer Society; Atlanta, GA: 2012.

(3). Green MR, Manikhas GM, Orlov S, Afanasyev B, Makhson AM, Bhar P, Hawkins MJ. Abraxane, a novel Cremophor-free, albumin-bound particle form of paclitaxel for the treatment of advanced non-small-cell lung cancer. Ann. Oncol. 2006; 17(8):1263–1268. [PubMed: 16740598]

(4). Hrkach J, Von Hoff D, Ali MM, Andrianova E, Auer J, Campbell T, De Witt D, Figa M, Figueiredo M, Horhota A, Low S, McDonnell K, Peeke E, Retnarajan B, Sabnis A, Schnipper E, Song JJ, Song YH, Summa J, Tompsett D, Troiano G, Van Geen Hoven T, Wright J, LoRusso P, Kantoff PW, Bander NH, Sweeney C, Farokhzad OC, Langer R, Zale S. Preclinical Development and Clinical Translation of a PSMA-Targeted Docetaxel Nanoparticle with a Differentiated Pharmacological Profile. Sci. Transl. Med. 2012; 4(128):128ra39.

(5). Kim DW, Kim SY, Kim HK, Kim SW, Shin SW, Kim JS, Park K, Lee MY, Heo DS. Multicenter phase II trial of Genexol-PM, a novel Cremophor-free, polymeric micelle formulation of paclitaxel, with cisplatin in patients with advanced non-small-cell lung cancer. Ann. Oncol. 2007; 18(12):2009–2014. [PubMed: 17785767]

(6). Gradishar WJ, Tjulandin S, Davidson N, Shaw H, Desai N, Bhar P, Hawkins M, O'Shaughnessy J. Phase III trial of nanoparticle albumin-bound paclitaxel compared with polyethylated castor oil-based paclitaxel in women with breast cancer. J. Clin. Oncol. 2005; 23(31):7794–803. [PubMed: 16172456]

(7). Schiller JH, Harrington D, Belani CP, Langer C, Sandler A, Krook J, Zhu J, Johnson DH. Comparison of Four Chemotherapy Regimens for Advanced Non-Small-Cell Lung Cancer. N. Engl. J. Med. 2002; 346(2):92–98. [PubMed: 11784875]

(8). O'Brien ME, Wigler N, Inbar M, Rosso R, Grischke E, Santoro A, Catane R, Kieback DG, Tomczak P, Ackland SP, Orlandi F, Mellars L, Alland L, Tendler C. Reduced cardiotoxicity and comparable efficacy in a phase III trial of pegylated liposomal doxorubicin HCl (CAELYX/Doxil) versus conventional doxorubicin for first-line treatment of metastatic breast cancer. Ann. Oncol. 2004; 15(3):440–449. [PubMed: 14998846]

(9). Boddy AV, Plummer ER, Todd R, Sludden J, Griffin M, Robson L, Cassidy J, Bissett D, Bernareggi A, Verrill MW, Calvert AH. A phase I and pharmacokinetic study of paclitaxel poliglumex (XYOTAX), investigating both 3-weekly and 2-weekly schedules. Clin. Cancer Res. 2005; 11(21):7834–7840. [PubMed: 16278406]

(10). Paz-Ares L, Ross H, O'Brien M, Riviere A, Gatzemeier U, Von Pawel J, Kaukel E, Freitag L, Digel W, Bischoff H, Garcia-Campelo R, Iannotti N, Reiterer P, Bover I, Prendiville J, Eisenfeld AJ, Oldham FB, Bandstra B, Singer JW, Bonomi P. Phase III trial comparing paclitaxel poliglumex vs docetaxel in the second-line treatment of non-small-cell lung cancer. Br. J. Cancer. 2008; 98(10):1608–1613. [PubMed: 18475293]

(11). Weiss GJ, Chao J, Neidhart JD, Ramanathan RK, Bassett D, Neidhart JA, Choi CH, Chow W, Chung V, Forman SJ, Garmey E, Hwang J, Kalinoski DL, Koczywas M, Longmate J, Melton RJ, Morgan R, Oliver J, Peterkin JJ, Ryan JL, Schluep T, Synold TW, Twardowski P, Davis ME, Yen Y. First-in-human phase 1/2a trial of CRLX101, a cyclodextrin-containing polymer-camptothecin nanopharmaceutical in patients with advanced solid tumor malignancies. Invest. New Drugs. 2013; 31(4):986–1000. [PubMed: 23397498]

(12). Hamaguchi T, Kato K, Yasui H, Morizane C, Ikeda M, Ueno H, Muro K, Yamada Y, Okusaka T, Shirao K, Shimada Y, Nakahama H, Matsumura Y. A phase I and pharmacokinetic study of NK105, a paclitaxel-incorporating micellar nanoparticle formulation. Br. J. Cancer. 2007; 97(2):170–176. [PubMed: 17595665]

(13). Lee KS, Chung HC, Im SA, Park YH, Kim CS, Kim SB, Rha SY, Lee MY, Ro J. Multicenter phase II trial of Genexol-PM, a Cremophor-free, polymeric micelle formulation of paclitaxel, in patients with metastatic breast cancer. Breast Cancer Res. Treat. 2008; 108(2):241–250. [PubMed: 17476588]

(14). Allen TM, Cullis PR. Drug Delivery Systems: Entering the Mainstream. Science. 2004; 303(5665):1818–1822. [PubMed: 15031496]

(15). Wiernik PH, Schwartz EL, Strauman JJ, Dutcher JP, Lipton RB, Paietta E. Phase I clinical and pharmacokinetic study of taxol. Cancer Res. 1987; 47(9):2486–2493. [PubMed: 2882837]

(16). Nyman DW, Campbell KJ, Hersh E, Long K, Richardson K, Trieu V, Desai N, Hawkins MJ, Von Hoff DD. Phase I and pharmacokinetics trial of ABI-007, a novel nanoparticle formulation of paclitaxel in patients with advanced nonhematologic malignancies. J. Clin. Oncol. 2005; 23(31):7785–7793. [PubMed: 16258082]

(17). Kim TY, Kim DW, Chung JY, Shin SG, Kim SC, Heo DS, Kim NK, Bang YJ. Phase I and pharmacokinetic study of Genexol-PM, a cremophor-free, polymeric micelle-formulated paclitaxel, in patients with advanced malignancies. Clin. Cancer Res. 2004; 10(11):3708–3716. [PubMed: 15173077]

(18). Maeda H. The enhanced permeability and retention (EPR) effect in tumor vasculature: the key role of tumor-selective macromolecular drug targeting. Adv. Enzyme Regul. 2001; 41(1):189–207. [PubMed: 11384745]

(19). Matsumura Y, Maeda H. A New Concept for Macromolecular Therapeutics in Cancer Chemotherapy: Mechanism of Tumoritropic Accumulation of Proteins and the Antitumor Agent Smancs. Cancer Res. 1986; 46(12 Part 1):6387–6392. [PubMed: 2946403]

(20). Lammers T, Hennink WE, Storm G. Tumour-targeted nanomedicines: principles and practice. Br. J. Cancer. 2008; 99(3):392–397. [PubMed: 18648371]

(21). Lammers T, Kiessling F, Hennink WE, Storm G. Nanotheranostics and image-guided drug delivery: current concepts and future directions. Mol. Pharmaceutics. 2010; 7(6):1899–1912.

(22). Sottoriva A, Spiteri I, Piccirillo SGM, Touloumis A, Collins VP, Marioni JC, Curtis C, Watts C, Tavaré S. Intratumor heterogeneity in human glioblastoma reflects cancer evolutionary dynamics. Proc. Natl. Acad. Sci. U.S.A. 2013; 110(10):4009–4014. [PubMed: 23412337]

(23). Eisenhauer EA, Therasse P, Bogaerts J, Schwartz LH, Sargent D, Ford R, Dancey J, Arbuck S, Gwyther S, Mooney M, Rubinstein L, Shankar L, Dodd L, Kaplan R, Lacombe D, Verweij J. New response evaluation criteria in solid tumours: Revised RECIST guideline (version 1.1). Eur. J. Cancer. 2009; 45(2):228–247. [PubMed: 19097774]

(24). Bigbee, W.; Herberman, RB. Tumor Markers and Immunodiagnosis. In: Kufe, DW.; Pollock, RE.; Weichselbaum, RR.; Bast, RC.; Gansler, TS.; Holland, JF.; Frei, E., editors. Cancer Medicine. 6th ed.. BC Decker; Hamilton, Ontario: 2003. p. 209-220.

(25). Kaestner SA, Sewell GJ. Chemotherapy Dosing Part I: Scientific Basis for Current Practice and Use of Body Surface Area. Clin. Oncol. 2007; 19(1):23–37.

(26). Al-Jamal WT, Kostarelos K. Liposomes: From a Clinically Established Drug Delivery System to a Nanoparticle Platform for Theranostic Nanomedicine. Acc. Chem. Res. 2011; 44(10):1094–1104. [PubMed: 21812415]

(27). Caldorera-Moore ME, Liechty WB, Peppas NA. Responsive Theranostic Systems: Integration of Diagnostic Imaging Agents and Responsive Controlled Release Drug Delivery Carriers. Acc. Chem. Res. 2011; 44(10):1061–1070. [PubMed: 21932809]

(28). Cole AJ, Yang VC, David AE. Cancer theranostics: the rise of targeted magnetic nanoparticles. Trends Biotechnol. 2011; 29(7):323–332. [PubMed: 21489647]

(29). Janib SM, Moses AS, MacKay JA. Imaging and drug delivery using theranostic nanoparticles. Adv. Drug Delivery Rev. 2010; 62(11):1052–1063.

(30). Lammers T, Aime S, Hennink WE, Storm G, Kiessling F. Theranostic nanomedicine. Acc. Chem. Res. 2011; 44(10):1029–1038. [PubMed: 21545096]

(31). Majumdar D, Peng XH, Shin DM. The medicinal chemistry of theragnostics, multimodality imaging and applications of nanotechnology in cancer. Curr. Top. Med. Chem. 2010; 10(12):1211–26. [PubMed: 20388107]

(32). Paulmurugan R, Oronsky B, Brouse CF, Reid T, Knox S, Scicinski J. Real Time Dynamic Imaging and Current Targeted Therapies in the War on Cancer: A New Paradigm. Theranostics. 2013; 3(6):437–447. [PubMed: 23781290]

(33). Dames P, Gleich B, Flemmer A, Hajek K, Seidl N, Wiekhorst F, Eberbeck D, Bittmann I, Bergemann C, Weyh T, Trahms L, Rosenecker J, Rudolph C. Targeted delivery of magnetic aerosol droplets to the lung. Nat. Nanotechnol. 2007; 2(8):495–499. [PubMed: 18654347]

(34). Cole AJ, David AE, Wang J, Galbán CJ, Yang VC. Magnetic brain tumor targeting and biodistribution of long-circulating PEG-modified, cross-linked starch-coated iron oxide nanoparticles. Biomaterials. 2011; 32(26):6291–6301. [PubMed: 21684593]

(35). Heesakkers RA, Jager GJ, Hovels AM, de Hoop B, van den Bosch HC, Raat F, Witjes JA, Mulders PF, van der Kaa CH, Barentsz JO. Prostate cancer: detection of lymph nodemetastases outside the routine surgical area with ferumoxtran-10-enhanced MR imaging. Radiology. 2009; 251(2):408–414. [PubMed: 19401573]

(36). Dilnawaz F, Singh A, Mohanty C, Sahoo SK. Dual drug loaded superparamagnetic iron oxide nanoparticles for targeted cancer therapy. Biomaterials. 2010; 31(13):3694–3706. [PubMed: 20144478]

(37). Ling Y, Wei K, Luo Y, Gao X, Zhong S. Dual docetaxel/ superparamagnetic iron oxide loaded nanoparticles for both targeting magnetic resonance imaging and cancer therapy. Biomaterials. 2011; 32(29):7139–7150. [PubMed: 21726899]

(38). Kim D, Jeong YY, Jon S. A Drug-Loaded Aptamer-Gold Nanoparticle Bioconjugate for Combined CT Imaging and Therapy of Prostate Cancer. ACS Nano. 2010; 4(7):3689–3696. [PubMed: 20550178]

(39). Liu Z, Chen K, Davis C, Sherlock S, Cao Q, Chen X, Dai H. Drug Delivery with Carbon Nanotubes for In vivo Cancer Treatment. Cancer Res. 2008; 68(16):6652–6660. [PubMed: 18701489]

(40). Liu Z, Sun X, Nakayama-Ratchford N, Dai H. Supra-molecular Chemistry on Water-Soluble Carbon Nanotubes for Drug Loading and Delivery. ACS Nano. 2007; 1(1):50–56. [PubMed: 19203129]

(41). Welsher K, Liu Z, Sherlock SP, Robinson JT, Chen Z, Daranciang D, Dai H. A route to brightly fluorescent carbon nanotubes for near-infrared imaging in mice. Nat. Nanotechnol. 2009; 4(11): 773–780. [PubMed: 19893526]

(42). Welsher K, Sherlock SP, Dai H. Deep-tissue anatomical imaging of mice using carbon nanotube fluorophores in the second near-infrared window. Proc. Natl. Acad. Sci. U.S.A. 2011; 108(22): 8943–8948. [PubMed: 21576494]

(43). Bagalkot V, Zhang L, Levy-Nissenbaum E, Jon S, Kantoff PW, Langer R, Farokhzad OC. Quantum Dot-Aptamer Conjugates for Synchronous Cancer Imaging, Therapy, and Sensing of Drug Delivery Based on Bi-Fluorescence Resonance Energy Transfer. Nano Lett. 2007; 7(10): 3065–3070. [PubMed: 17854227]

(44). Gao X, Cui Y, Levenson RM, Chung LWK, Nie S. In vivo cancer targeting and imaging with semiconductor quantum dots. Nat. Biotechnol. 2004; 22(8):969–976. [PubMed: 15258594]

(45). Huang CK, Lo CL, Chen HH, Hsiue GH. Multifunctional Micelles for Cancer Cell Targeting, Distribution Imaging, and Anticancer Drug Delivery. Adv. Funct. Mater. 2007; 17(14):2291–2297.

(46). Kim S, Lim C-K, Na J, Lee Y-D, Kim K, Choi K, Leary JF, Kwon IC. Conjugated polymer nanoparticles for biomedical in vivo imaging. Chem. Commun. 2010; 46(10):1617–1619.

(47). Wu C, Bull B, Szymanski C, Christensen K, McNeill J. Multicolor Conjugated Polymer Dots for Biological Fluorescence Imaging. ACS Nano. 2008; 2(11):2415–2423. [PubMed: 19206410]

(48). Davis ME. Design and development of IT-101, a cyclodextrin-containing polymer conjugate of camptothecin. Adv. Drug Delivery Rev. 2009; 61(13):1189–1192.

(49). Schluep T, Hwang J, Hildebrandt IJ, Czernin J, Choi CH, Alabi CA, Mack BC, Davis ME. Pharmacokinetics and tumor dynamics of the nanoparticle IT-101 from PET imaging and tumor histological measurements. Proc. Natl. Acad. Sci. U.S.A. 2009; 106(27):11394–11399. [PubMed: 19564622]

(50). Young C, Schluep T, Hwang J, Eliasof S. CRLX101 (formerly IT-101)-A Novel Nanopharmaceutical of Camptothecin in Clinical Development. Curr. Bioact. Compd. 2011; 7(1):8–14. [PubMed: 22081768]

(51). Rapoport N, Nam K-H, Gupta R, Gao Z, Mohan P, Payne A, Todd N, Liu X, Kim T, Shea J, Scaife C, Parker DL, Jeong E-K, Kennedy AM. Ultrasound-mediated tumor imaging and nanotherapy using drug loaded, block copolymer stabilized perfluor-ocarbon nanoemulsions. J. Controlled Release. 2011; 153(1):4–15.

(52). Diamond KR, Malysz PP, Hayward JE, Patterson MS. Quantification of fluorophore concentration in vivo using two simple fluorescence-based measurement techniques. J. Biomed. Opt. 2005; 10(2):024007. [PubMed: 15910081]

(53). Mourant JR, Johnson TM, Los G, Bigio IJ. Non-invasive measurement of chemotherapy drug concentrations in tissue: preliminary demonstrations of in vivo measurements. Phys. Med. Biol. 1999; 44(5):1397–1417. [PubMed: 10368027]

(54). Palmer GM, Boruta RJ, Viglianti BL, Lan L, Spasojevic I, Dewhirst MW. Non-invasive monitoring of intra-tumor drug concentration and therapeutic response using optical spectroscopy. J. Controlled Release. 2010; 142(3):457–464.

(55). Reif R, Wang M, Joshi S, A'Amar O, Bigio IJ. Optical method for real-time monitoring of drug concentrations facilitates the development of novel methods for drug delivery to brain tissue. J. Biomed. Opt. 2007; 12(3):034036. [PubMed: 17614744]

(56). Saager RB, Cuccia DJ, Saggese S, Kelly KM, Durkin AJ. Quantitative fluorescence imaging of protoporphyrin IX through determination of tissue optical properties in the spatial frequency domain. J. Biomed. Opt. 2011; 16(12):126013. [PubMed: 22191930]

(57). Chen H, Moore T, Qi B, Colvin DC, Jelen EK, Hitchcock DA, He J, Mefford OT, Gore JC, Alexis F, Anker JN. Monitoring pH-Triggered Drug Release from Radioluminescent Nanocapsules with X-ray Excited Optical Luminescence. ACS Nano. 2013; 7(2):1178–1187. [PubMed: 23281651]

(58). Koo H, Lee H, Lee S, Min KH, Kim MS, Lee DS, Choi Y, Kwon IC, Kim K, Jeong SY. In vivo tumor diagnosis and photodynamic therapy via tumoral pH-responsive polymeric micelles. Chem. Commun. 2010; 46(31):5668–5670.

(59). Tian G, Ren W, Yan L, Jian S, Gu Z, Zhou L, Jin S, Yin W, Li S, Zhao Y. Red-Emitting Upconverting Nanoparticles for Photodynamic Therapy in Cancer Cells Under Near-Infrared Excitation. Small. 2013; 9(11):1929–1938. [PubMed: 23239556]

(60). Viglianti BL, Ponce AM, Michelich CR, Yu D, Abraham SA, Sanders L, Yarmolenko PS, Schroeder T, MacFall JR, Barboriak DP, Colvin OM, Bally MB, Dewhirst MW. Chemodosimetry of in vivo tumor liposomal drug concentration using MRI. Magn. Reson. Med. 2006; 56(5):1011–1018. [PubMed: 17029236]

(61). Cunin F, Schmedake TA, Link JR, Li YY, Koh J, Bhatia SN, Sailor MJ. Biomolecular screening with encoded porous-silicon photonic crystals. Nat. Mater. 2002; 1(1):39–41. [PubMed: 12618846]

(62). Wu EC, Andrew JS, Cheng L, Freeman WR, Pearson L, Sailor MJ. Real-time monitoring of sustained drug release using the optical properties of porous silicon photonic crystal particles. Biomaterials. 2011; 32(7):1957–1966. [PubMed: 21122914]

(63). Doan VV, Sailor MJ. Luminescent Color Image Generation on Porous Silicon. Science. 1992; 256(5065):1791–1792. [PubMed: 17743033]

(64). Park J-H, Gu L, von Maltzahn G, Ruoslahti E, Bhatia SN, Sailor MJ. Biodegradable luminescent porous silicon nano-particles for in vivo applications. Nat. Mater. 2009; 8(4):331–336. [PubMed: 19234444]

(65). de Boer WDAM, Timmerman D, Dohnalova K, Yassievich IN, Zhang H, Buma WJ, Gregorkiewicz T. Red spectral shift and enhanced quantum efficiency in phonon-free photoluminescence from silicon nanocrystals. Nat. Nanotechnol. 2010; 5(12):878–884. [PubMed: 21113157]

(66). Erogbogbo F, Yong K-T, Roy I, Hu R, Law W-C, Zhao W, Ding H, Wu F, Kumar R, Swihart MT, Prasad PN. In Vivo Targeted Cancer Imaging, Sentinel Lymph Node Mapping and Multi-Channel Imaging with Biocompatible Silicon Nanocrystals. ACS Nano. 2010; 5(1):413–423. [PubMed: 21138323]

(67). Gu L, Park J-H, Duong KH, Ruoslahti E, Sailor MJ. Magnetic Luminescent Porous Silicon Microparticles for Localized Delivery of Molecular Drug Payloads. Small. 2010; 6(22):2546–2552. [PubMed: 20814923]

(68). Mik EG, Johannes T, Zuurbier CJ, Heinen A, Houben-Weerts JHPM, Balestra GM, Stap J, Beek JF, Ince C. In Vivo Mitochondrial Oxygen Tension Measured by a Delayed Fluorescence Lifetime Technique. Biophy. J. 2008; 95(8):3977–3990.

(69). Jarvi MT, Niedre MJ, Patterson MS, Wilson BC. Singlet Oxygen Luminescence Dosimetry (SOLD) for Photodynamic Therapy: Current Status, Challenges and Future Prospects. Photochem. Photobiol. 2006; 82(5):1198–1210. [PubMed: 16808593]

(70). Niedre MJ, Yu CS, Patterson MS, Wilson BC. Singlet oxygen luminescence as an in vivo photodynamic therapy dose metric: validation in normal mouse skin with topical amino-levulinic acid. Br. J. Cancer. 2005; 92(2):298–304. [PubMed: 15655542]

(71). Cheong WF, Prahl SA, Welch AJ. A review of the optical properties of biological tissues. IEEE J. Quantum Electron. 1990; 26(12):2166–2185.

(72). Savla R, Taratula O, Garbuzenko O, Minko T. Tumor targeted quantum dot-mucin 1 aptamer-doxorubicin conjugate for imaging and treatment of cancer. J. Controlled Release. 2011; 153(1):16–22.

(73). Hampl J, Hall M, Mufti NA, Yao Y.-m. M. MacQueen DB, Wright WH, Cooper DE. Upconverting Phosphor Reporters in Immunochromatographic Assays. Anal. Biochem. 2001; 288(2):176–187. [PubMed: 11152588]

(74). Ukonaho T, Rantanen T, Jämsen L, Kuningas K, Päkkilä H, Lövgren T, Soukka T. Comparison of infrared-excited up-converting phosphors and europium nanoparticles as labels in a two-site immunoassay. Anal. Chim. Acta. 2007; 596(1):106–115. [PubMed: 17616247]

(75). Petoral RM, Söderlind F, Klasson A, Suska A, Fortin MA, Abrikossova N, Selegård L, Käll P-O, Engström M, Uvdal K. Synthesis and Characterization of Tb3+-Doped Gd2O3 Nanocrystals: A

Bifunctional Material with Combined Fluorescent Labeling and MRI Contrast Agent Properties. J. Phys. Chem. C. 2009; 113(17):6913–6920.

(76). Mader HS, Kele P, Saleh SM, Wolfbeis OS. Upconverting luminescent nanoparticles for use in bioconjugation and bioimaging. Curr. Opin. Chem. Biol. 2010; 14(5):582–596. [PubMed: 20829098]

(77). Xu Z, Gao Y, Huang S, Ma P, Lin J, Fang J. A luminescent and mesoporous core-shell structured Gd2O3: Eu(3+)@nSiO2@mSiO2 nanocomposite as a drug carrier. Dalton Trans. 2011; 40(18): 4846–4854. [PubMed: 21431226]

(78). Capozzi V, Perna G, Carmone P, Gallone A, Lastella M, Mezzenga E, Quartucci G, Ambrico M, Augelli V, Biagi PF, Ligonzo T, Minafra A, Schiavulli L, Pallara M, Cicero R. Optical and photoelectronic properties of melanin. Thin Solid Films. 2006; 511-512(0):362–366.

(79). Sarna, T.; Swartz, HA. The Physical Properties of Melanins. In: Nordlung, JJ.; Boissy, RE.; Hearing, VJ.; King, RA.; Oetting, WS.; Ortonne, JP., editors. The Pigmentary System: Physiology and Pathophysiology. 2nd edition. Oxford University Press; New York: 1998. p. 311-341.

(80). Ortonne JP. Photoprotective properties of skin melanin. Br. J. Dermatol. 2002; 146(s61):7–10. [PubMed: 11966725]

(81). de Gruijl FR, van Kranen HJ, Mullenders LHF. UV-induced DNA damage, repair, mutations and oncogenic pathways in skin cancer. J. Photochem. Photobiol., B. 2001; 63(1-3):19–27. [PubMed: 11684448]

(82). Stolik S, Delgado JA, Pérez A, Anasagasti L. Measurement of the penetration depths of red and near infrared light in human "ex vivo" tissues. J. Photochem. Photobiol., B. 2000; 57(2-3):90–93. [PubMed: 11154088]

(83). Chen H, Colvin DC, Qi B, Moore T, He J, Mefford OT, Alexis F, Gore JC, Anker JN. Magnetic and optical properties of multifunctional core-shell radioluminescence nanoparticles. J. Mater. Chem. 2012; 22(25):12802–12809. [PubMed: 24520183]

(84). Gai S, Yang P, Li C, Wang W, Dai Y, Niu N, Lin J. Synthesis of Magnetic, Up-Conversion Luminescent, and Mesoporous Core-Shell-Structured Nanocomposites as Drug Carriers. Adv. Funct. Mater. 2010; 20(7):1166–1172.

(85). Kang X, Cheng Z, Li C, Yang D, Shang M, Ma PÄ, Li G, Liu N, Lin J. Core-Shell Structured Up-Conversion Luminescent and Mesoporous NaYF4:Yb3+/Er3+@nSiO2@mSiO2 Nanospheres as Carriers for Drug Delivery. J. Phys. Chem. C. 2011; 115(32):15801–15811.

(86). Sun C, Pratx G, Carpenter CM, Liu H, Cheng Z, Gambhir SS, Xing L. Synthesis and Radioluminescence of PEGylated Eu3+-doped Nanophosphors as Bioimaging Probes. Adv. Mater. 2011; 23(24):H195–H199. [PubMed: 21557339]

(87). Champion JA, Mitragotri S. Role of target geometry in phagocytosis. Proc. Natl. Acad. Sci. U.S.A. 2006; 103(13):4930–4934. [PubMed: 16549762]

(88). Geng Y, Dalhaimer P, Cai S, Tsai R, Tewari M, Minko T, Discher DE. Shape effects of filaments versus spherical particles in flow and drug delivery. Nat. Nanotechnol. 2007; 2(4):249–255. [PubMed: 18654271]

(89). Huang X, Li L, Liu T, Hao N, Liu H, Chen D, Tang F. The shape effect of mesoporous silica nanoparticles on biodistribution, clearance, and biocompatibility in vivo. ACS Nano. 2011; 5(7): 5390–5399. [PubMed: 21634407]

(90). Ntziachristos V. Going deeper than microscopy: the optical imaging frontier in biology. Nat. Methods. 2010; 7(8):603. [PubMed: 20676081]

(91). Xu CT, Svenmarker P, Liu H, Wu X, Messing ME, Wallenberg LR, Andersson-Engels S. High-Resolution Fluorescence Diffuse Optical Tomography Developed with Nonlinear Upconverting Nanoparticles. ACS Nano. 2012; 6(6):4788–4795. [PubMed: 22568960]

(92). Carpenter CM, Sun C, Pratx G, Rao R, Xing L. Hybrid x-ray/optical luminescence imaging: characterization of experimental conditions. Med. Phys. 2010; 37(8):4011–4018. [PubMed: 20879562]

(93). Carpenter CM, Pratx G, Sun C, Xing L. Limited-angle x-ray luminescence tomography: methodology and feasibility study. Phys. Med. Biol. 2011; 56(12):3487. [PubMed: 21606553]

(94). Chen D, Zhu S, Yi H, Zhang X, Chen D, Liang J, Tian J. Cone beam x-ray luminescence computed tomography: A feasibility study. Med. Phys. 2013; 40(3):031111–14. [PubMed: 23464291]

(95). Edelman RR, Warach S. Magnetic Resonance Imaging. N. Engl. J. Med. 1993; 328(10):708–716. [PubMed: 8433731]

(96). Lee, DC.; Carroll, TJ. Magnetic Resonance Iimaging. In Practical Signal and Image Processing in Clinical Cardiology. Goldberger, JJ.; Ng, J., editors. Springer; London: 2010. p. 251-273.

(97). Jun YW, Lee JH, Cheon J. Chemical design of nanoparticle probes for high-performance magnetic resonance imaging. Angew. Chem., Int. Ed. Engl. 2008; 47(28):5122–5135. [PubMed: 18574805]

(98). Ponce AM, Viglianti BL, Yu D, Yarmolenko PS, Michelich CR, Woo J, Bally MB, Dewhirst MW. Magnetic Resonance Imaging of Temperature-Sensitive Liposome Release: Drug Dose Painting and Antitumor Effects. J. Natl. Cancer Inst. 2007; 99(1):53–63. [PubMed: 17202113]

(99). Abraham SA, Edwards K, Karlsson G. r. MacIntosh S, Mayer LD, McKenzie C, Bally MB. Formation of transition metal-doxorubicin complexes inside liposomes. Biochim. Biophys. Acta, Biomembr. 2002; 1565(1):41–54.

(100). Viglianti BL, Abraham SA, Michelich CR, Yarmolenko PS, MacFall JR, Bally MB, Dewhirst MW. In vivo monitoring of tissue pharmacokinetics of liposome/drug using MRI: Illustration of targeted delivery. Magn. Reson. Med. 2004; 51(6):1153–1162. [PubMed: 15170835]

(101). Needham D, Anyarambhatla G, Kong G, Dewhirst MW. A New Temperature-sensitive Liposome for Use with Mild Hyper-thermia: Characterization and Testing in a Human Tumor Xenograft Model. Cancer Res. 2000; 60(5):1197–1201. [PubMed: 10728674]

(102). Crossgrove J, Zheng W. Manganese toxicity upon over-exposure. NMR Biomed. 2004; 17(8): 544–553. [PubMed: 15617053]

(103). Parenti M, Rusconi L, Cappabianca V, Parati EA, Groppetti A. Role of dopamine in manganese neurotoxicity. Brain Res. 1988; 473(2):236–240. [PubMed: 2852985]

(104). Lentschig MG, Reimer P, Rausch-Lentschig UL, Allkemper T, Oelerich M, Laub G. Breath-hold gadolinium-enhanced MR angiography of the major vessels at 1.0 T: dose-response findings and angiographic correlation. Radiology. 1998; 208(2):353–357. [PubMed: 9680558]

(105). de Smet M, Langereis S, den Bosch S. v. Grüll H. Temperature-sensitive liposomes for doxorubicin delivery under MRI guidance. J. Controlled Release. 2010; 143(1):120–127.

(106). de Smet M, Heijman E, Langereis S, Hijnen NM, Grüll H. Magnetic resonance imaging of high intensity focused ultrasound mediated drug delivery from temperature-sensitive liposomes: An in vivo proof-of-concept study. J. Controlled Release. 2011; 150(1):102–110.

(107). Tagami T, Foltz WD, Ernsting MJ, Lee CM, Tannock IF, May JP, Li SD. MRI monitoring of intratumoral drug delivery and prediction of the therapeutic effect with a multifunctional thermosensitive liposome. Biomaterials. 2011; 32(27):6570–6578. [PubMed: 21641639]

(108). Negussie AH, Yarmolenko PS, Partanen A, Ranjan A, Jacobs G, Woods D, Bryant H, Thomasson D, Dewhirst MW, Wood BJ, Dreher MR. Formulation and characterisation ofmagnetic resonance imageable thermally sensitive liposomes for use with magnetic resonance-guided high intensity focused ultrasound. Int. J. Hyperthermia. 2011; 27(2):140–155. [PubMed: 21314334]

(109). Santra S, Jativa SD, Kaittanis C, Normand G, Grimm J, Perez JM. Gadolinium-encapsulating iron oxide nanoprobe as activatable NMR/MRI contrast agent. ACS Nano. 2012; 6(8):7281–7294. [PubMed: 22809405]

(110). Hardman R. A toxicologic review of quantum dots: toxicity depends on physicochemical and environmental factors. Environ. Health Perspect. 2006; 114(2):165–172. [PubMed: 16451849]

(111). Derfus AM, Chan WCW, Bhatia SN. Probing the Cytotoxicity of Semiconductor Quantum Dots. Nano Lett. 2003; 4(1):11–18.

(112). Ye L, Yong K-T, Liu L, Roy I, Hu R, Zhu J, Cai H, Law W-C, Liu J, Wang K, Liu J, Liu Y, Hu Y, Zhang X, Swihart MT, Prasad PN. A pilot study in non-human primates shows no adverse response to intravenous injection of quantum dots. Nat. Nanotechnol. 2012; 7(7):453–458. [PubMed: 22609691]

(113). Yong K-T, Law W-C, Hu R, Ye L, Liu L, Swihart MT, Prasad PN. Nanotoxicity assessment of quantum dots: from cellular to primate studies. Chem. Soc. Rev. 2013; 42(3):1236–1250. [PubMed: 23175134]

(114). Liu J, Erogbogbo F, Yong K-T, Ye L, Liu J, Hu R, Chen H, Hu Y, Yang Y, Yang J, Roy I, Karker NA, Swihart MT, Prasad PN. Assessing Clinical Prospects of Silicon Quantum Dots: Studies in Mice and Monkeys. ACS Nano. 2013; 7(8):7303–7310. [PubMed: 23841561]

(115). Cobley CM, Chen J, Cho EC, Wang LV, Xia Y. Gold nanostructures: a class of multifunctional materials for biomedical applications. Chem. Soc. Rev. 2011; 40(1):44–56. [PubMed: 20818451]

(116). Abraham GE, Himmel PB. Management of Rheumatoid Arthritis: Rationale for the Use of Colloidal Metallic Gold. J. Nutr. Environ. Med. 1997; 7(4):295–305.

(117). The Research Sub-Committee of the Empire Rheumatism Council. Gold Therapy in Rheumatoid Arthritis: Final Report of a Multicentre Controlled Trial. Ann. Rheum. Dis. 1961; 20(4):315–334. [PubMed: 18623862]

(118). Stroh A, Zimmer C, Gutzeit C, Jakstadt M, Marschinke F, Jung T, Pilgrimm H, Grune T. Iron oxide particles for molecular magnetic resonance imaging cause transient oxidative stress in rat macrophages. Free Radical Biol. Med. 2004; 36(8):976–84. [PubMed: 15059638]

(119). Chu KS, Hasan W, Rawal S, Walsh MD, Enlow EM, Luft JC, Bridges AS, Kuijer JL, Napier ME, Zamboni WC, DeSimone JM. Plasma, tumor and tissue pharmacokinetics of Docetaxel delivered via nanoparticles of different sizes and shapes in mice bearing SKOV-3 human ovarian carcinoma xenograft. Nano-medicine (New York, NY, U.S.). 2013; 9(5):686–693.

(120). Perrault SD, Walkey C, Jennings T, Fischer HC, Chan WCW. Mediating Tumor Targeting Efficiency of Nanoparticles Through Design. Nano Lett. 2009; 9(5):1909–1915. [PubMed: 19344179]

(121). Kostarelos K, Bianco A, Prato M. Promises, facts and challenges for carbon nanotubes in imaging and therapeutics. Nat. Nanotechnol. 2009; 4(10):627–633. [PubMed: 19809452]

(122). Poland CA, Duffin R, Kinloch I, Maynard A, Wallace WAH, Seaton A, Stone V, Brown S, MacNee W, Donaldson K. Carbon nanotubes introduced into the abdominal cavity of mice show asbestos-like pathogenicity in a pilot study. Nat. Nanotechnol. 2008; 3(7):423–428. [PubMed: 18654567]

(123). Schipper ML, Nakayama-Ratchford N, Davis CR, Wong Shi Kam N, Chu P, Zhuang L, Xiaoming S, Hongjie D, Gambhir SS. A pilot toxicology study of single-walled carbon nanotubes in a small sample of mice. Nat. Nanotechnol. 2008; 3(4):216–221. [PubMed: 18654506]

(124). Bai Y, Zhang Y, Zhang J, Mu Q, Zhang W, Butch ER, Snyder SE, Yan B. Repeated administrations of carbon nanotubes in male mice cause reversible testis damage without affecting fertility. Nat. Nanotechnol. 2010; 5(9):683–689. [PubMed: 20693989]

(125). Lacerda L, Ali-Boucetta H, Herrero MA, Pastorin G, Bianco A, Prato M, Kostarelos K. Tissue histology and physiology following intravenous administration of different types of function-alized multiwalled carbon nanotubes. Nanomedicine (London, U.K.). 2008; 3(2):149–161.

(126). Singh R, Pantarotto D, Lacerda L, Pastorin G, Klumpp C. d. Prato M, Bianco A, Kostarelos K. Tissue biodistribution and blood clearance rates of intravenously administered carbon nanotube radiotracers. Proc. Natl. Acad. Sci. U.S.A. 2006; 103(9):3357–3362. [PubMed: 16492781]

(127). Murray AR, Kisin ER, Tkach AV, Yanamala N, Mercer R, Young SH, Fadeel B, Kagan VE, Shvedova AA. Factoring-in agglomeration of carbon nanotubes and nanofibers for better prediction of their toxicity versus asbestos. Part. Fibre Toxicol. 2012; 9:10. [PubMed: 22490147]

(128). Tang ACL, Hwang G-L, Tsai S-J, Chang M-Y, Tang ZCW, Tsai M-D, Luo C-Y, Hoffman AS, Hsieh PCH. Biosafety of Non-Surface Modified Carbon Nanocapsules as a Potential Alternative to Carbon Nanotubes for Drug Delivery Purposes. PLoS One. 2012; 7(3):e32893. [PubMed: 22457723]

(129). Connor EE, Mwamuka J, Gole A, Murphy CJ, Wyatt MD. Gold Nanoparticles Are Taken Up by Human Cells but Do Not Cause Acute Cytotoxicity. Small. 2005; 1(3):325–327. [PubMed: 17193451]

(130). Niidome T, Yamagata M, Okamoto Y, Akiyama Y, Takahashi H, Kawano T, Katayama Y, Niidome Y. PEG-modified gold nanorods with a stealth character for in vivo applications. J. Controlled Release. 2006; 114(3):343–347.

(131). Hale GM, Querry MR. Optical Constants of Water in the 200-nm to 200-μm Wavelength Region. Appl. Opt. 1973; 12(3):555–563. [PubMed: 20125343]

(132). Lim YT, Kim S, Nakayama A, Stott NE, Bawendi MG, Frangioni JV. Selection of quantum dot wavelengths for biomedical assays and imaging. Mol. Imaging. 2003; 2(1):50–64. [PubMed: 12926237]

(133). Smith AM, Mancini MC, Nie S. Bioimaging: Second window for in vivo imaging. Nat Nanotechnol. 2009; 4(11):710–711. [PubMed: 19898521]

(134). Won N, Jeong S, Kim K, Kwag J, Park J, Kim SG, Kim S. Imaging depths of near-infrared quantum dots in first and second optical windows. Mol. Imaging. 2012; 11(4):338–352. [PubMed: 22954148]

(135). Weissleder R. A clearer vision for in vivo imaging. Nat. Biotechnol. 2001; 19(4):316–317. [PubMed: 11283581]

(136). Li YY, Cunin F, Link JR, Gao T, Betts RE, Reiver SH, Chin V, Bhatia SN, Sailor MJ. Polymer Replicas of Photonic Porous Silicon for Sensing and Drug Delivery Applications. Science. 2003; 299(5615):2045–2047. [PubMed: 12663921]

(137). Dolmans DEJGJ, Fukumura D, Jain RK. Photodynamic therapy for cancer. Nat. Rev. Cancer. 2003; 3(5):380–387. [PubMed: 12724736]

(138). Burgess P, Hutt PB, Farokhzad OC, Langer R, Minick S, Zale S. On firm ground: IP protection of therapeutic nanoparticles. Nat. Biotechnol. 2010; 28(12):1267–1270. [PubMed: 21139609]

(139). Kirkpatrick DL, Weiss M, Naumov A, Bartholomeusz G, Weisman RB, Gliko O. Carbon Nanotubes: Solution for the Therapeutic Delivery of siRNA? Materials. 2012; 5(2):278–301.

(140). O'Neal DP, Hirsch LR, Halas NJ, Payne JD, West JL. Photo-thermal tumor ablation in mice using near infrared-absorbing nanoparticles. Cancer Lett. 2004; 209(2):171–176. [PubMed: 15159019]

(141). Schwartz JA, Shetty AM, Price RE, Stafford RJ, Wang JC, Uthamanthil RK, Pham K, McNichols RJ, Coleman CL, Payne JD. Feasibility study of particle-assisted laser ablation of brain tumors in orthotopic canine model. Cancer Res. 2009; 69(4):1659–1667. [PubMed: 19208847]

(142). Schwartz JA, Price RE, Gill-Sharp KL, Sang KL, Khorchani J, Goodwin BS, Payne JD. Selective nanoparticle-directed ablation of the canine prostate. Lasers Surg. Med. 2011; 43(3):213–220. [PubMed: 21412805]

(143). Libutti SK, Paciotti GF, Byrnes AA, Alexander HR, Gannon WE, Walker M, Seidel GD, Yuldasheva N, Tamarkin L. Phase I and Pharmacokinetic Studies of CYT-6091, a Novel PEGylated Colloidal Gold-rhTNF Nanomedicine. Clin. Cancer Res. 2010; 16(24):6139–6149. [PubMed: 20876255]

(144). Bourrinet P, Bengele HH, Bonnemain B, Dencausse A, Idee JM, Jacobs PM, Lewis JM. Preclinical safety and pharmacokinetic profile of ferumoxtran-10, an ultrasmall super-paramagnetic iron oxide magnetic resonance contrast agent. Invest. Radiol. 2006; 41(3):313–324. [PubMed: 16481915]

(145). Sharma R, Saini S, Ros PR, Hahn PF, Small WC, de Lange EE, Stillman AE, Edelman RR, Runge VM, Outwater EK, Morris M, Lucas M. Safety profile of ultrasmall super-paramagnetic iron oxide ferumoxtran-10: phase II clinical trial data. J. Magn. Reson. Imaging. 1999; 9(2):291–294. [PubMed: 10077027]

(146). Willmann JK, van Bruggen N, Dinkelborg LM, Gambhir SS. Molecular imaging in drug development. Nat. Rev. Drug Discovery. 2008; 7:591–607.

(147). Gerd M, Joel SK. Positron emission tomography. Phys. Med. Biol. 2006; 51(13):R117. [PubMed: 16790899]

(148). Li Z, Conti PS. Radiopharmaceutical chemistry for positron emission tomography. Adv. Drug Delivery Rev. 2010; 62(11):1031–1051.
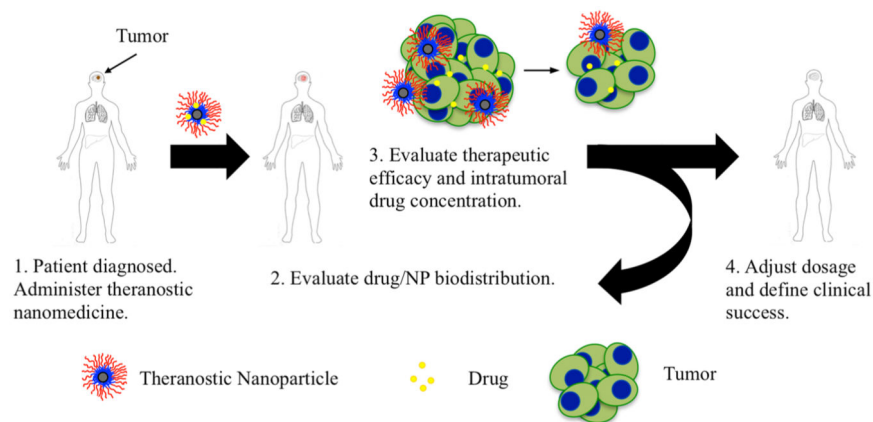
Figure 1.
Theranostic nanomedicine with real-time monitoring of drug biodistribution, in situ concentration, and therapeutic effcacy would provide tools to clinicians to monitor therapeutic effcacy and adjust treatment regimens accordingly.
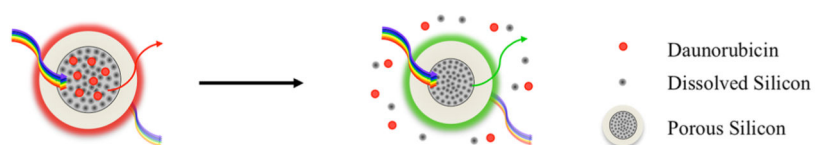
Figure 2.
Porous silicon (PSi) particles can be loaded with daunorubicin via covalent conjugation. PSi particles exhibit narrow reflectance spectra, and when loaded with drug reflect visible light at approximately 660 nm. However, dissolution of the porous silicon results in the release of daunorubicin and orthosilicate species. This resulted in a blue shift of the reflectance spectrum which was directly correlated to the amount of daunorubicin released.
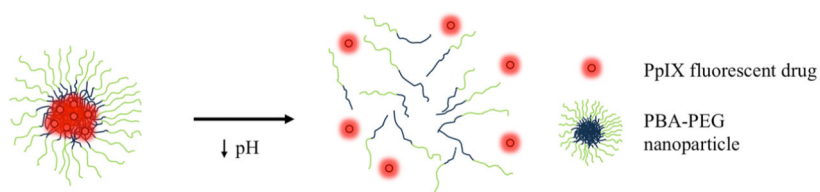
Figure 3.
pH-sensitive PBA-PEG nanoparticles are loaded with the photoactive drug protoporphyrin IX (PpIX). This drug also has a fluorescent spectrum, and measuring fluorescent signal in tissue can quantitate the relative amount of drug. Decrease in intratumoral pH causes protonation of PBA which results in destabilization of the nanoparticle and release of PpIX.
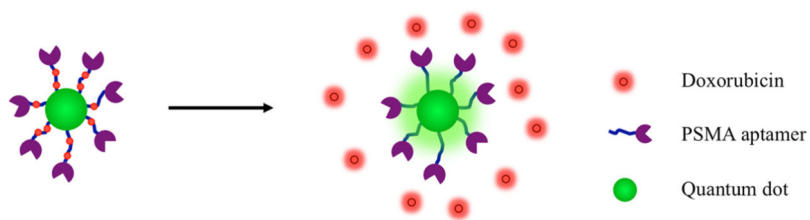
Figure 4.
Bifluorescence resonance energy transfer enables the measure of drug loading onto quantum dot–aptamer conjugates. Doxorubicin, a fluorescent anticancer drug, binds the prostate cancer targeting aptamer. Doxorubicin quenches the fluorescent signal from the quantum dot, and the targeting aptamer quenches fluorescence from doxorubicin. Upon release, both entities regain their fluorescence.
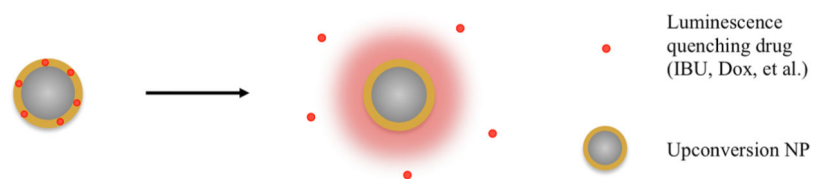
Figure 5.
Here nanoparticle visible light luminescence, which may be excited by NIR light, is attenuated by loaded drug. As drug is released, nanoparticle luminescence returns. These systems enable quantitative measure of drug release.
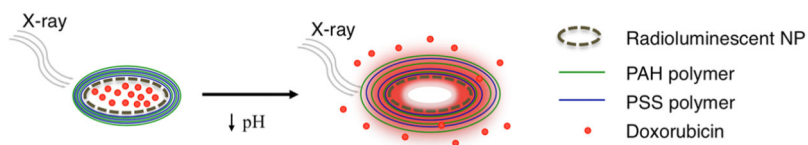
Figure 6.
Radioluminescent Gd_2O_2S nanoparticles doped with terbium and europium
(Gd_2O_2S:Tb/Eu) were coated layer by layer with poly(styrenesulfonate sodium) (PSS) and
poly(allyl-amine HCl) (PAH). These hollow nanoparticles were able to encapsulate
doxorubicin and exhibit pH dependent response. Doxorubicin attenuates radioluminescence.
Luminescence returns in intensity proportional to doxorubicin release.
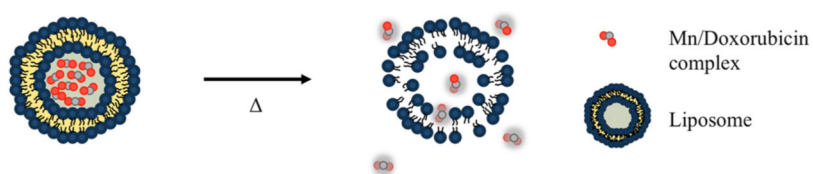
Figure 7.
Thermally sensitive liposomes are destabilized when temperature is increased. This results in the release of manganese–doxorubicin complexes that are measured via T_1-weighted magnetic resonance imaging.
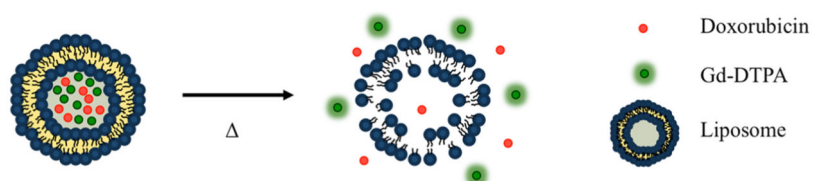
Figure 8.
Temperature-sensitive liposomes also encapsulated the imaging agent Gd-DTPA and anticancer drug doxorubicin. Upon application of heat, liposome integrity is ruptured which releases both drug and imaging agent. Gd-DTPA concentration was measured via MRI and approximated Dox concentrations in tissue.
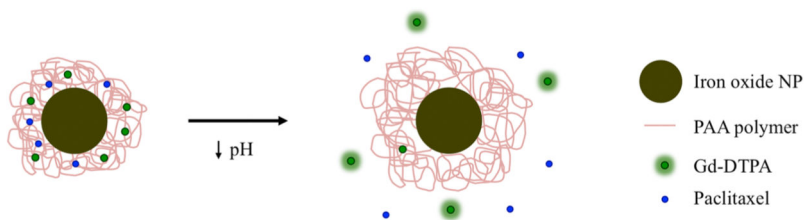
Figure 9.
Iron oxide nanoparticles coated with poly(acrylic acid) (PAA) were loaded with paclitaxel and Gd-DTPA. When encapsulated within the PAA matrix, the MRI contrast agent Gd-DTPA was effectively turned off by the iron oxide NP. However, upon release, Gd-DTPA enhanced T_1 contrast. Paclitaxel and Gd-DTPA release was pH dependent because acidic pH caused PAA to swell and degrade.

Table 1

Summary of Methods for Measuring the Release of Drug from Particles

Method/Contrast Agent	Advantages	Limitations	Ref.
Reflection spectroscopy: Porous silicon photonic crystals change color upon drug release	• Biodegradable • Tunable pore size/surface chemistry	• Reflection spectrum not observable through thick tissue	61-67

Fluorescent drug accumulation/singlet oxygen luminescence	• Simple to use	• Poor deep tissue monitoring
		  ○ Autofluorescence
		  ○ Light attenuation in tissue.
		  ○ Spatial resolution is limited by optical scattering.
			58, 68-70

Fluorescent nanoparticles	• Low cost
	• Possibly portable
	• Quantitative release
		• Poor deep tissue monitoring
		  ○ Autofluorescence
		  ○ Light attenuation in tissue
		  ○ Spatial resolution is limited by optical scattering.
			43, 72, 77

Upconverting nanoparticles	• High photostability • Low toxicity • Good tissue penetration depth • No autofluorescence	• Spatial resolution of image is limited by optical scattering.	59, 84, 85
Radioluminescent nanoparticles	• No autofluorescence • High spatial resolution images • Deep soft tissue penetration	• X-ray dose limits detection depth and image resolution • Poor deep tissue monitoring ○ Light attenuation in tissue Spectral distortion due to wavelength-dependent attenuation.	57, 83
Temperature-sensitive liposomes loaded with a drug-MRI/T_1 contrast agent complex	• No depth limitation • Sensitive • Quantitative • Temperature-triggered system • Good spatial resolution	• Cost of MRI instrument • Potential Mn^{2+} ion associated toxicity	60, 98, 99, 100
Temperature-sensitive liposomes co-encapsulate drug and MRI/ T_1 contrast agent	• No depth limitation • Sensitive • Good spatial resolution • Quantitative. • Temperature-triggered system	• Cost of MRI instrument • Released drug molecules PK/PD behavior different than MRI contrast agent	104-108
Coated iron oxide NP loaded with Gd-DTPA	• No depth limitation • Sensitive	• Cost of MRI instrument	109

Method/Contrast Agent	Advantages	Limitations	Ref.
MRI/T_1 contrast agent	• Quantitative • pH-triggered system • Good spatial resolution	• Released drug molecules PK/PD behavior different than MRI contrast agent • Release kinetics of drug and Gd-DTPA are different.	